

TSPO imaging in animal models of brain diseases

Nadja van Camp, Sonia Lavisse, Pauline Roost, Francesco Gubinelli, Ansel Hillmer, Hervé Boutin

▶ To cite this version:

Nadja van Camp, Sonia Lavisse, Pauline Roost, Francesco Gubinelli, Ansel Hillmer, et al.. TSPO imaging in animal models of brain diseases. European Journal of Nuclear Medicine and Molecular Imaging, 2021, 49 (1), pp.77-109. 10.1007/s00259-021-05379-z . cea-04470964

HAL Id: cea-04470964 https://cea.hal.science/cea-04470964

Submitted on 21 Feb 2024

HAL is a multi-disciplinary open access archive for the deposit and dissemination of scientific research documents, whether they are published or not. The documents may come from teaching and research institutions in France or abroad, or from public or private research centers.

L'archive ouverte pluridisciplinaire **HAL**, est destinée au dépôt et à la diffusion de documents scientifiques de niveau recherche, publiés ou non, émanant des établissements d'enseignement et de recherche français ou étrangers, des laboratoires publics ou privés.

REVIEW ARTICLE



TSPO imaging in animal models of brain diseases

Nadja Van Camp ¹ • Sonia Lavisse ¹ • Pauline Roost ¹ • Francesco Gubinelli ¹ • Ansel Hillmer ^{2,3,4} • Hervé Boutin ^{5,6,7} •

Received: 1 March 2021 / Accepted: 25 April 2021 / Published online: 10 July 2021 © The Author(s) 2021

Abstract

Over the last 30 years, the 18-kDa TSPO protein has been considered as the PET imaging biomarker of reference to measure increased neuroinflammation. Generally assumed to image activated microglia, TSPO has also been detected in endothelial cells and activated astrocytes. Here, we provide an exhaustive overview of the recent literature on the TSPO-PET imaging (i) in the search and development of new TSPO tracers and (ii) in the understanding of acute and chronic neuroinflammation in animal models of neurological disorders. Generally, studies testing new TSPO radiotracers against the prototypic [11C]-R-PK11195 or more recent competitors use models of acute focal neuroinflammation (e.g. stroke or lipopolysaccharide injection). These studies have led to the development of over 60 new tracers during the last 15 years. These studies highlighted that interpretation of TSPO-PET is easier in acute models of focal lesions, whereas in chronic models with lower or diffuse microglial activation, such as models of Alzheimer's disease or Parkinson's disease, TSPO quantification for detection of neuroinflammation is more challenging, mirroring what is observed in clinic. Moreover, technical limitations of preclinical scanners provide a drawback when studying modest neuroinflammation in small brains (e.g. in mice). Overall, this review underlines the value of TSPO imaging to study the time course or response to treatment of neuroinflammation in acute or chronic models of diseases. As such, TSPO remains the gold standard biomarker reference for neuroinflammation, waiting for new radioligands for other, more specific targets for neuroinflammatory processes and/or immune cells to emerge.

Keywords Translocator protein 18 kDa · Neuroinflammation · Alzheimer's disease · Parkinson's disease · Stroke · Multiple sclerosis · Positron emission tomography

This article is part of the Topical Collection on Preclinical Imaging.

- Hervé Boutin
 herve.boutin@manchester.ac.uk
- Université Paris-Saclay, CEA, CNRS, MIRCen, Laboratoire des Maladies Neurodégénératives, 92265 Fontenay-aux-Roses, France
- Department of Psychiatry, Yale School of Medicine, New Haven, CT, USA
- Department of Radiology & Biomedical Imaging, Yale School of Medicine, New Haven, CT, USA
- Department of Biomedical Engineering, Yale School of Engineering & Applied Science, New Haven, CT, USA
- Division of Neuroscience and Experimental Psychology, School of Biological Sciences, Faculty of Brain and Mental Health, University of Manchester, M13 9PL, Manchester, UK
- Wolfson Molecular Imaging Centre, University of Manchester, 27 Palatine Road, M20 3LJ Manchester, UK
- Geoffrey Jefferson Brain Research Centre, Manchester Academic Health Science Centre, Northern Care Alliance & University of Manchester, Manchester, UK

General introduction

Nowadays, the 18-kDa translocator protein (18-kDa TSPO) is the most prominent biomarker for imaging of glial activation and has been reviewed more than a hundred times over the last two decades (cf. PubMed search terms: "(omega* OR TSPO OR PBR OR PK11195) AND (PET OR positron) AND (brain OR cereb*) AND (English[lang])" and selecting "review" or "systematic review"). About 40 years ago, this protein was named peripheral benzodiazepine receptors (or omega-3 binding site) due to its pharmacology (high affinity for some benzodiazepines) and its preferential expression in the myocardium, kidney and adrenals [1–3]. Its overexpression in brain lesions rapidly identified this protein as a potential in vivo imaging marker of inflammation-related neurodegeneration, notably in models of brain ischaemia [4-8]. One of the first applications of TSPO/PBR radioligands for positron emission tomography (PET) imaging was to image brain tumours in man [9, 10]. It was only in the mid- to late 1990s,



using animal models of brain diseases that an increased level of TSPO/PBR was proven to be associated with microglial activation [11–14]. Preclinical models are of great utility when it comes to testing, validating and implementing new biomarkers, imaging methods and contrast agents. The preclinical contribution in the development of new radioligands for TSPO here is no exception, as underlined by its representation in the literature – more than a third of the abovementioned reviews.

Our aim here is to provide an exhaustive overview of the recent literature on the use of animal models in two major applications in the field of preclinical TSPO-PET imaging: either as a tool to develop new tracers and/or imaging methodologies or as a model to understand the contribution of acute and chronic neuroinflammation in neurological disorder models.

Models of acute neuroinflammation

Tracer development

The animal models of acute neuroinflammation described below have mostly been used for the development and validation of TSPO tracers as they provide generally a consistent, robust and focal neuroinflammatory response and TSPO expression with a well-described time course. From a tracer development perspective, on top of classical brain tracer characteristics such as high blood-brain barrier penetrance, neuroinflammation and TSPO tracers have specific highly desirable characteristics that are summarized in Table 1.

P-gp, P-glycoprotein; N/A, not applicable

Lipopolysaccharide (LPS) model

LPS, also referred to as endotoxin, is a major component of the outer membrane of gram-negative bacteria, with lipid A in the membrane and the O antigen constituting the outer-facing surface of the bacterium. Soluble endotoxin is released when bacteria are destroyed but is also released physiologically as outer membrane vesicles [15]. LPS is a potent inducer of inflammation both in peripheral tissues and in the central nervous system via the activation of toll-like receptor 4 (TLR4), which results in NF-kB transcriptional activation of hundreds of inflammatory genes, including pro-inflammatory cytokines such as TNFα, IL-6 and pro-IL-1β. LPS administration in preclinical models is performed systematically (intravenous, i.v., or intraperitoneal, i.p.) or by stereotactic intracerebral injection. In this topic, we will discuss TSPO-PET imaging studies in models using both administration routes. We used the following search in PubMed, "(omega* OR TSPO OR PBR OR PK11195) AND (PET OR positron) AND (brain OR cereb*) AND (LPS OR lipopolysaccharide) AND (rat OR mouse OR mice OR animal* OR experimental OR pig OR gerbil OR rabbit OR guinea OR primate OR dog OR cat) AND (English[lang])", which returned initially 27 records. After exclusion of those that were not PET imaging studies that used LPS as a comorbidity factor and those not using LPS as a model per se, 18 references were retained to TSPO-PET imaging in LPS models.

It has been a matter of discussion how peripherally administered LPS induces neuroinflammation in the central nervous system. Initially, it was suggested that LPS-induced neuroinflammation was an indirect effect through TNF α , which crosses the blood-brain barrier [16]. However, it has been shown more recently that LPS infiltrates the brain via lipoprotein receptor (such as SR-B1) transport in which LPS binds specifically to those receptors at the blood-brain interfaces [17]. These receptors are located in astrocytes (as part of immunologic functional barriers), tanycytes that are in direct contact with the cerebrospinal fluid along the ventricular walls and centrum ventricular organs) and endothelial cells (arbitrating a neuroimmune communication by actively responding to immune challenges such as LPS through the release of cytokines and other mechanisms) [17]. Cytokine production and direct interaction of LPS with TLR4 induce microglial activation, the first-line defence of the brain. Using adult mice receiving a single intraperitoneal administration of LPS (1 mg/kg), it has been demonstrated by in vitro immunohistochemical studies

Table 1 Required characteristics for new neuroinflammation and TSPO tracers

Challenges for new neuroinflammation tracers	Specific requirements for new TSPO tracers
High metabolic stability	
High free ligand availability in plasma (i.e., low binding to circ	ulating cells or proteins)
High brain availability (i.e., high blood-brain barrier penetrance	e, not <i>P-gp</i> substrate)
N/A	No sensitivity to the TSPO rs6971 polymorphism
Development of cell-specific ligands: microglia vs astrocytes	N/A
Neuroinflammatory phenotypic selectivity: pro- vs anti-inflammatory	N/A



that microglial proliferation occurs nonuniformly in the central nervous system but in a region- and dose-dependent manner. This is followed by a return to control levels 20 days after a single stimulation independent of the LPS dose (100 µg/kg or 1 mg/kg LPS) [18]. Altogether, various studies confirm that acute systemic LPS administration induces transient inflammation in the central nervous system [19, 20, 15], which makes LPS an appealing approach to measure the "neuroimmune response" by imaging TSPO levels. Moreover, at a low dose, the pro-inflammatory properties of endotoxin mimic the complex responses to systemic infection. However, due to the transient effect of acute endotoxin, consistent timing of imaging is required to ensure consistent results. Ota et al. were the first to image the neuroinflammatory response after a systematic LPS administration in the rat brain (2mg/kg, i.p.) using [11C]-R-PK11195 [21]. Animals were scanned before and 2 days after LPS administration, and the difference in SUV uptake was estimated with voxel-wise statistical parametric mapping. This revealed a striato-cortical cluster, which surprisingly reflected a significant decrease of the TSPO-PET signal rather than an increase. As this result was not further supported by any ex vivo or in vitro data, additionally considering both the limitations of the SUV measure in the absence of any blood data and the low specificity of [11C]-R-PK11195, interpretation of these data needs to be considered cautiously. A far more complete study in the rat brain was performed by Schmidt et al., who evaluated the time and regional course of the [11C]PBR28 TSPO-PET signal after a systemic (i.p.) LPS challenge (3 mg/kg) in the context of a genetic risk factor for Parkinson's disease (more details in the paragraph "Parkinson's disease" below) [22]. This study reported a reliable and consistent neuroinflammatory response 24 h after the challenge as visualized by in vitro autoradiography using [11C]PBR28. Subsequently, a longitudinal in vivo [11C]PBR28 PET study demonstrated a significant detectable LPS-induced TSPO-PET response 10 months after administration, particularly in the cortical and ventral regions. As such, TSPO response to peripheral inflammation can also be monitored in an ethically viable manner by minimizing pathogenic risk to human subjects, providing an important model for studying immune signalling in human research [23]. TSPO imaging can leverage this model by conducting scans before and after endotoxin challenge, to measure the change in TSPO brain levels. The results provide important information on the brain's immune response to a stimulus, or immune function, to complement the snapshots of the brain's neuroimmune state assessed by single baseline TSPO scans. Such endotoxin protocol was first applied to non-human primates (baboons), where serial [11C]PBR28 images were acquired after i.v. administration of 0.1-mg/kg endotoxin [24]. This dose increased the [11 C]PBR28 volume of distribution (V_T) by +29% and +62% relative to baseline 1 h and 4 h after endotoxin injection, respectively. These results demonstrated the time dependence of measurements of endotoxin effects. The peak response occurred 3–5 h post-dose, which informed the design for future human studies. In humans, acute endotoxin administration (1.0 ng/kg LPS, i.v.) induced a 30–60% increase in [11 C]PBR28 V_T in the brain 3 h after injection [25]. In the rhesus monkeys, a similar dose (1.0 ng/kg LPS, i.v.) increased [11 C]PBR28 V_T by +39% from baseline 2.5 h post-endotoxin [26].

Altogether, a comparison across different TSPO-PET studies after the LPS challenge highlights an important species difference in the LPS sensitivity. Globally 2.5 to 4 h, a comparable TSPO response (+40 to +60% increase) after LPS challenge could be observed in baboon, rhesus NHP, and human, but the LPS dose administered in baboon was 10⁵-fold higher compared to the doses in rhesus or human. Importantly, both the baboon and human studies demonstrated that TSPO-PET brain changes after endotoxin challenge were accompanied with changes in subjective sickness behaviour and blood levels of inflammatory cytokines. In the rodent, even higher doses (in the order of mg/kg) are needed to evoke a detectable neuroinflammatory TSPO response (of note, the administration route in rodents is i.p. vs i.v. in NHP and humans). Altogether, this suggests that rhesus monkeys and humans exhibit greater sensitivity to endotoxin compared to rodents and baboons.

The neuroinflammatory response to systemic endotoxin depends on more factors. A study on mice systematically treated with LPS (0.63 mg/kg) revealed significant age and sex influences, which were reflected by both differential expression of pro-inflammatory factors and an increased ex vivo TSPO ligand uptake, using [18F]VC701, in aged female mice [27]. Furthermore, the brain regions displayed differential susceptibility to LPS, which is attributable to the number of microglia present and the levels of inflammation-related factors produced by these cells [28]. As such, the systemic endotoxin model can provide valuable new insight on the role of inflammation in the pathogenesis of brain diseases such as stroke, and Parkinson's disease, which will be discussed in the next chapters. LPS-induced systemic inflammation was further used to evaluate the influence on the [11C]-R-PK11195 TSPO-PET signal in the presence of a pre-existing neuroinflammatory lesion [29]. Here, the authors suggested that the TSPO-PET signal refers to the level of microglial activation rather than the number in activated microglia, an observation that was contradicted by Tournier et al. as discussed below [30]. Finally, Vignal et al. [31] used TSPO-PET imaging to evaluate the impact of immune regulating factors on brain [18F]FEPPA TSPO-PET response. An overview of the studies is presented in Table 2.

Intracerebral administered LPS *directly* interacts with TLR4 located on astrocytes and microglia, hence locally activating pro-inflammatory microglia and astrocytes. Neurotoxic reactive astrocytes can also be activated *indirectly* through pro-inflammatory factors expressed by microglia [32]. Even



 Table 2
 Overview of TSPO imaging studies in different LPS models

PET/SPECT tracer	Rational	LPS model	Species	Imaging time point	Major outcomes and additional readouts	Ref.
[¹⁸ F]FEPPA	Optimization of radiosynthesis; impact of astroglial connexin 43 (Cx43) on brain immunoregulation	Systemic administration (5 mg/kg, i.p.) Cx43 ^{fl/fl} /hGFAP-Cre; Cx43 ^{fl/fl} model	C57Bl/6J mice	24 h post-injection	 Systemic inflammation results in two-fold increase in TSPO-PET. Deletion of astrocyte Cx43 abolishes the LPS-induced TSPO 	[45, 31]
[¹¹ C]-R-PK11195	Impact of systemic inflammation on toxic-induced neuroinflammation	Systemic administration (10 mg/kg, i.p.) after intracerebral ethanol-induced neuroinflammation	Rats	4 days post-injection	increase LPS induced higher TSPO-PET signal. The number of activated microglia in the neurotoxic lesion is similar in both conditions. LPS induced higher expression of inflammatory	[29]
[¹⁸ F]VC701	Evaluation of age and sex differences	Systemic administration (0.63 mg/kg)	C57Bl/6J mice	6 h post-injection	cytokines Pro-inflammatory response in aged female is higher compared to adult female and aged male	[27]
[¹¹ C]PBR28	To evaluate the impact of systemic inflammation on TSPO-PET in the brain; development of a paradigm to measure dynamic microglial changes in the NHP brain	Systemic administration: 0.1 mg/kg, i.v., and 1 ng/kg, i.v.	NHP: baboon Rhesus mon- key	1–5.5 h and ~22 h post-injection 2.5 h, 14 days post-injection	LPS-induced systemic inflammation produces a detectable TSPO-PET signal in the brain mediated by inflammatory cytokines. The colony-stimulating factor 1 receptor kinase inhibitor depletes brain microglia and induces a significant decrease in the TSPO-PET signal, which recovers after 12 days	[26, 24]
[¹¹ C]PBR28	To evaluate the impact of systemic inflammation on TSPO-PET in the brain	Systemic administration (1 ng/kg, i.v.)	Human	3h	First in a human demonstration that a systemic LPS challenge induces microglial activation in the brain	[25, 46]
[¹¹ C]-R-PK11195	Model of maternal infection as a risk factor for periventricular leukomalacia and cerebral palsy (CP)	Intra-uterine exposure in pregnant rabbits (20 µg/kg)	Rabbit	1–7 days post-injection	Increased TSPO-PET in the brain and increased inflammatory markers are detected up to 2 weeks after	[47]
[¹⁸ F]DPA-713	in neonates To evaluate if TSPO-TEP reveals specifically the pro- or	Cultured rodent astrocytes, microglia and macrophages	Mice		birth TSPO expression corresponds to a pro-inflammatory phenotype	[33]



Table 2 (continued)

PET/SPECT tracer	Rational	LPS model	Species	Imaging time point	Major outcomes and additional readouts	Ref.
	anti-inflammatory phenotype	stimulated with TNF, LPS and IL-4; mice injected with AdTNF or IL-4				
[¹²³ I]CLINDE	Determine the cell population in which TSPO is altered using fluorescence activated cell sorting on radioligand-treated tissue	Intracerebral (hippocampus) (10 µg)	Rat	3 days post-injection	LPS induces a microglial expansion and an increase in microglial TSPO binding	[30]
[11C]-R-PK11195, [11C]DAA1106, [11C]PBR28, [18F]DPA-714, [18F]GE-180, [18F]fluoromethyl-PB-R28 48–51, 34, 52]	Validation and comparison of TSPO-PET ligands; validation of pharmacokinetic quantification models	Intracerebral (striatum) (1 μg, 10 μg, 50 μg)	Rat	3–4 days post-injection/- longitudinal after injection	2nd generation TSPO ligands reveal a higher uptake compared to that of [11C]-R-PK11195. IHC characterization of the LPS model	[40, 35, 38, 44, 39,
[¹⁸ F]CB251	Comparison and validation of a new 3rd generation TSPO ligand; characterization and identification of immune cells contributing to LPS-induced neuroinflammation	Intracerebral (striatum) (5 µg/2 µl)	Mice	4 days post-injection	[18F]CB251 does not show a differential affinity for the TSPO polymorphism; following LPS-induced neuroinflammation, peripheral immune cells cross the BBB and actively contribute to the TSPO-PET signal. Bioluminescence studies to identify the contribution of peripheral immune cells to the brain immune response	[37]

though both pro-inflammatory microglia and astrocytes contribute to the LPS-induced TSPO-PET signal [33–35, 30], microglia are abundantly present over astrocytes, suggesting that the TSPO-PET signal in the intracerebral induced LPS model is mainly due to an increase in microglial density. In vitro studies demonstrated that LPS slightly decreased TSPO gene expression in human microglia and [3H]PBR28 binding sites in human macrophages [36]. Building on these findings, an innovative ex vivo technique using fluorescence-activated cell sorting of radioligand-treated tissue reported that while LPS did not change radioactivity per cell in microglia, LPS dramatically increased the number of microglia per gram of tissue [30]. Despite possible LPS binding to endothelial

cells [17], there is no evidence for changes in TSPO levels in endothelial cells following LPS stimulation [33]. Based on the robust imaging [25] and immunohistochemistry [34] literature reporting LPS-induced increases in TSPO signal, findings point to LPS increasing the number of TSPO-expressing microglia and not the number of TSPO per microglia. TSPO imaging of acute LPS effects should be more accurately characterized as capturing "microglial proliferation", rather than assessing "microglial activation". A recent multimodal imaging study combining TSPO-PET and bioluminescence imaging demonstrated that peripheral immune cells cross the blood-brain barrier, exacerbate the LPS-induced neuroinflammation to produce higher levels of neurotoxicity and actively



contribute to the TSPO-PET signal. For this study, the authors used a new TSPO ligand, [18F]CB251, which has a higher affinity for TSPO compared to ligands such as PK11195, PBR28 and GE-180 [37]. In general, intracerebral induced neuroinflammation by LPS is an attractive experimental model to confirm or compare the sensitivity of new TSPO radioligands in a situation of acute immune activation in rodents [34, 38–40]. Additionally, this model is also used to evaluate new PET ligands specific for other proinflammatory microglial-specific targets, such as CB2 and P2X7, in comparison to validated TSPO ligands [35, 41]. A review of the literature highlights the important differences between experimental protocols in terms of injected dose, site of injection and the time point of imaging (Table 2). Intracerebral LPS doses vary from 1 [35, 40] to 5-10 µg [42, 43] and even up to 50 µg [34, 44]; injection is generally performed in the striatum but also in the hippocampus and substantia nigra; finally, imaging time points vary from hours to days or even weeks post-injection [42, 43]. These experimental differences undoubtedly affect the neuroinflammatory response and its imaging readout, rendering the comparison between studies almost impossible.

Stroke

Neuroinflammation was truly identified as an essential component of the pathophysiology of stroke in the mid- to late 1990s [53–55], although the identification of TSPO glial expression was originally described after cerebral ischaemia, when TSPO was still referred to as the peripheral benzodiazepine receptor [56, 7]. Only about 10-15 years later, those ex vivo observations in animal models were confirmed by in vivo PET imaging in clinical settings [57-59]. In 2015, Boutin and Pinborg published a review on the literature of TSPO-PET imaging in stroke covering brain ischaemia models and clinical studies [60]. Overall, that review [60] covered clinical studies investigating (i) TSPO after stroke using [11C]-R-PK11195 [58], (ii) preclinical studies in primates [61, 62] using a clinical scanner and [11C]-R-PK11195 as well as (iii) the first preclinical studies using small animal dedicated scanners. These studies aimed to evaluate – at the time – new tracers such as [11C]PBR28 [63] or [18F]DPA-714 [64] or better determine the time course of TSPO expression following focal ischemia [65]. Altogether, these first studies were extremely helpful to demonstrate the importance of neuroinflammation after stroke and the value of TSPO-PET imaging to quantify it, and they provided invaluable information in terms of the study design to future preclinical and clinical studies. Therefore, in the following paragraphs, we will only review the literature on TSPO imaging in stroke models that has been published since the most recent paper included in that review at the time of publication, which was Tiwari et al. [66]. For this section, we used the following search in PubMed, "(omega* OR TSPO OR PBR OR PK11195) AND (PET OR positron) AND (brain OR cereb*) AND (stroke OR ischem* OR ischaem*) AND (rat OR mouse OR mice OR animal* OR experimental OR pig OR gerbil OR rabbit OR guinea OR primate OR dog OR cat) AND (English[lang])", limiting the search to 2015–2021. This returned initially 52 records, excluding those not using stroke models, reviews and clinical research papers, and 26 references were finally kept for this section. The results of all these studies have been summarized in Table 3; most of them did confirm their in vivo PET results using immunohistochemistry and/or autoradiography, but these results will not be discussed in full details here; instead, a short summary of those ex vivo/in vitro results can be found in Table 3.

To test new TSPO tracers, stroke models present the advantages of being clinically relevant and to induce a strong TSPO+ microglial activation that has been demonstrated both preclinically [8, 11] and clinically [57, 58, 60]. In this context, Boutin et al. used a transient model of middle cerebral artery occlusion (MCAO) in rats to evaluate the then-new TSPO tracer [18F]GE-180 [67] and demonstrated a superior uptake, ipsi-/contralateral ratio and BP_{ND} for [18F]GE-180 when compared to [11C]-R-PK11195. This preclinical study and another using LPS-induced milder neuroinflammation [40] positively demonstrated the benefit in terms of the signal-to-noise ratio of [18F]GE-180 vs [11C]-R-PK11195. However, clinical studies demonstrated that, for reasons that remain unclear, the brain pharmacokinetics of [18F]GE-180 were slower – i.e. more than one could anticipate – and less favourable in man as those observed in rat. Despite this observation, several studies have recently shown the value of this tracer to measure neuroinflammation in vivo [68–73]. In the same line, Fujinaga et al. used a stroke model in rats to test and select new TSPO tracer candidates and identified that amongst those 2-(5-(6-[¹⁸F]fluoropyridin-3-yl)-2-oxobenzo[d]oxazol-3(2H)yl)-N-methyl-N-phenylacetamide (compound d in [74]) and [¹⁸F]5 (N-(4-[18F]fluorobenzyl)-N-methyl-2-(7-methyl-8oxo-2-phenyl-7,8-dihydro-9H-purin-9-yl)acetamide) [75] were the best candidates with better signal-to-noise ratio than [11C]-R-PK11195. Other TSPO tracers have been evaluated using stroke models, such as [18F]VUIIS1008 [76], [18F]VUIIS1008A [77] and [18F]F-DPA [78]. Generally, those new tracers showed potential with a better signal-tonoise ratio than that of [11C]-R-PK11195 that they aim to replace. However, the direct comparison of [18F]VUIIS1008 with [18F]DPA-714 revealed that [18F]VUIIS1008 yielded no gain in term of signal-to-noise ratio when compared to [¹⁸F]DPA-714, with similar ipsi- to contralateral ratio and BP_{ND} values. When comparing, a posteriori, data reported for [18F]VUIIS1008A, [18F]VUIIS1008 and [18F]DPA-714, the same group seemed to indicate that it was also the case for [18F]VUIIS1008A [77]. However, in a more recent study using [18F]VUIIS1008 and [18F]DPA-714, a significant



 Table 3
 Overview of the preclinical TSPO-PET studies in experimental stroke models (published since 2015 [60]).

PET tracer *	Rational	Stroke model and species	Imaging time points	Main imaging findings	Additional readouts	Ref.
[¹⁸ F]GE-180 [¹¹ C]-R-PK11195	Validation of [¹⁸ FJGE-180 as new TSPO tracer by direct comparison with [¹¹ CJ-R-PK11195	60-min intraluminal MCAO in male Wistar rats (357±44g)	5-6 days post-MCAO	• Better signal-to-noise ratio with ¹⁸ F GE-180; BP _{ND} =3.5±0.4 for ¹⁸ F GE-180 > BPND=2.4±0.5 for ¹¹ C -R-PK11195 • Percentage intact ¹⁸ F GE-180 in brain: 98±2%, 96±3% and 94±2% at 10, 30 and 60 min post-injection	PET and ARG: displacement by unlabelled R-PK11195 or GE-180) confirmed TSPO specificity and in vivo results	Moi imaging (202
[¹¹ C]-R-PK11195 2[¹⁸ F]-fluoro-A85380 (nAChR α4β2) [102]	Investigate the role of nAChR α4β2 in neuroinflammation; TSPO [¹¹ C]-R-PK11195 imaging used as reference biomarker/tracer	2-h intraluminal MCAO in male SD rats 1, 3, 7, 14, 21, and 28 (300 g) days post-MCAO		F]-fluoro-A85380 and 195 s 3–7 post-MCAO th tracer uptake at 14–28 days antagonist increased	PET results confirmed by IHC for nAChR $\alpha 4\beta 2$ and TSPO	[96]
[¹⁸ F]FEBMP	Evaluation of [¹⁸ F]FEBMP as new TSPO tracer	30-min intraluminal MCAO in 8–9-weeks-old (240–330 g) male SD rats	7 days post-MCAO	20±0.12 (BPND: 2.72 MP in the brain: 83.2 d 60 min post-injection	Human brain tissue ARG: no sensitivity of [¹⁸ FJFEBMP to TSPO rs6971 polymorphism (comparison with [¹¹ C]-R-PK11195, [¹¹ C]PBR28, [¹¹ C]AC-5216, and [¹¹ C]DAA1106)	[99]
[¹¹ C]-R-PK11195 (USPIO for detection of phagocytic cells)	Mapping of activated microglia 18 phagocytic cells	Permanent microsphere-induced MCAO in male Wistar rats (320–365 g)	PET at day 6, 27 and 55 USPIO MR at day 7, 27, 56	<u>s</u> +	PET and MR data confirmed by histological and IHC staining	[85]
[¹⁵ OJH ₂ O (CBF) [¹¹ CJ-R-PK11195 [¹⁸ FJFDG	Investigate the contribution of NI Permanent microspher to [¹⁸ F]FDG signal MCAO in male W (320–363 g)	Permanent microsphere-induced MCAO in male Wistar rats (320–363 g)	7 days pre-MCAo and at days 2, 7, 14, 21 and 42	urs principally in the ischemic brain region, ithout sufficient metabolic supply 'n mask even more severe hypometabolism as NI increases (1871) in the last of the	PET and T2 MR data confirmed by histology and IHC	[87]
[11C]-R-PK11195 [18F]FLT (NSC proliferation)	Investigate the effects of tDCS on NI and NSC proliferation	60-min intraluminal MCAO in male Wistar rats (290–330 g)	[18 FJFLT and [17 CJR-P-KI1195 at day 16 post-MCAO	(SC proliferation improvement but increased is secondary is seed the	T2 MR at day 2 post-MCAO to assess the success of MCAO, TSPO-PET confirmed by iba+ IHC	[100]
[¹⁸ FJDPA-714 [¹⁸ FJFSPG (system xc.) [103]	Better understanding of system xc in NI vs TSPO as reference biomarker for NI in stroke	90-min intraluminal MCAO in male SD rats (300 g)	Before and at 1, 3, 7, 14, 21 and 28 days post-MCAO	of microglia • [¹⁸ F]FSPG: increased uptake peaking at days 3 to 7, decreasing decreasing from days 14 to 28 post-MCAO	T2 MR 24 h post-MCAO to assess infarct size, PET data confirmed by IHC; system xc inhibitors reduced expression of M1 (TSPO, CCL2, TNF and iNOS) and increased arginase (M2) biomarkers	83

Table 3 (continued)						
PET tracer *	Rational	Stroke model and species	Imaging time points	Main imaging findings	Additional readouts	Ref.
[¹¹ CJ-R-PK11195 [¹⁸ FJFLT (NSC proliferation)	Investigate the role of TLR4 in neurogenesis and inflammation	Proximal (MCA bifurcation) in 2-3-months-old male C57BL/10 J (TLR4***) mice and distal MCAO (posterior branch) in C57BL/10ScNJ (TLR4***) mice	2, 7 and 14 days post-MCAO	from day 14 post-MCAO • xc inhibitors reduced [¹⁸ F]DPA-714 uptake at 7 days post-MCAO • Modest increase in [¹¹ C]-R-PKI1195 uptake 2 days post-MCAO in TLR4***, not in TLR4** mice • Similar increase in [¹¹ C]-R-PKI1195 uptake in TLR4*** and TLR4** mice at 7 days in TLR4** in TLR4** and TLR4** mice at 7 days in TLR4** bigher uptake of [¹⁸ F]FLT • Decreased uptake of [¹⁸ F]FLT	T2 MR 24 h post-MCAO to assess infarct size, PET data confirmed by IHC	[98]
[¹⁸ FJDPA-714	Investigate the role of NI in SAH Intraluminal ACA Wistar rats (30	Intraluminal ACA puncture in male Wistar rats (300–350 g)	2 days post-SAH	A-714 SUV r 14 uptake	In vivo PET data confirmed by [³ HJ-R-PK11195 autoradiography and IHC	[82]
[^{1,1} C]PBR28	Better understanding of NI in stroke disease mechanisms	90-min left MCAO (M2 segment) by microwire tip insertion through the ventral tail artery in SD rats (362±28 g)	1, 4, 7 and 14 days post-MCAO	ral pe	T2 MR before each PET acquisition, in vivo PET findings confirmed by CD11b, CD68, GFAP and TSPO IHC	[83]
Four new [¹⁸ F]-labelled acetamiidobenzoxazo- lone TSPO compounds	Selection of best TSPO tracer candidate	30-min intraluminal MCAO in male SD rats (7 weeks old, 220–240 g)	7 days post-MCAO	• No significant change in the contralateral side • Best compound: 2-(5-(6-1 ¹⁸ F)fluoropyridin-3-yl)-2-oxobenzo [d]oxazol-3(2H)-yl)-N-methyl-N-phenylacetamide (compound d) with and ipsl-/contralateral ratio of	C6 glioma model in rats (ipsi-/contralateral ratio, 4.20±1.09; BP _{ND} , 2.29±079); ARG confirmed in vivo PET	[74]
[¹¹ CJ-R-PK11195 and [¹¹ CJNE40 (CB2 receptors) [104]	Evaluation of [11 C]NE40 and CB2 receptor as marker of early microglial activation	Photothrombotic left MCAO in 8-weeks-old male SD rats (250-300 g)	24h post-MCAO	4.20 ± 0.37 and BP _{ND} of 2.33 ± 0.25 • No significant increase in [¹¹ C]NE40 BP _{ND} and in the ipsilateral increase in [¹¹ C]NE40 BP _{ND} and in the ipsilateral	IHC confirmed the absence of TSPO 24 h post-MCAO; CB2 staining colocalized with a variety of cells positive for CD11b, Neuly and NG2 continued.	[93]
[¹⁸ FJVUIIS1008 [¹⁸ FJDPA-714	Comparison of new TSPO tracer [18F]VUIIS1008 with [18F]DPA-714	Comparison of new TSPO tracer 90-min intraluminal MCAO in male SD [$^{\rm I8}{\rm FJVMIS1008}$ with rats (296±9 g) [$^{\rm I8}{\rm FJDPA-714}$	Before and at 1, 3, 7, 14, 21 and 28 days post-MCAO		Infact size confirmed to be similar for both tracers. • Microglial/macrophage cellular localization of TSPO confirmed by CD11b IHC	[76]
[¹⁸ F]F-DPA	Radiochemistry and preliminary evaluation of a novel TSPO tracer: [^{1/8} FJF-DPA ([^{1/8} FJDPA-714 derivative)	30-min intraluminal MCAO in SD rats 7 days post-MCAO	7 days post-MCAO	unlabelled VUIIS1008 with DPA-714 at 1 mg/kg • Ipsi- to contralateral ratio: 4.26±0.34 at 90min post-injection • Ipsilateral BP _{ND} : 4.02±1.32		[87]
[''F]GE180						- 8



PET tracer *	Rational	Stroke model and species	Imaging time points	Main imaging findings	Additional readouts	Ref.
	Evaluate microglial activation after global perinatal hypoxic injury	Hypoxia resuscitation in newborn Noroc piglets (12–36 h old) + 1 positive control (LPS injected)	Baseline and 0–5 h, 6–8 h, 24–26 h and 29–32 h after hypoxia/ resuscitation	 Hypoxia resuscitation did not increase [¹⁸F]GE180 uptake in any of the brain regions measured LPS induced an increase in [¹⁸F]GE180 uptake in the LPS-injected basal ganglia 	Post-mortem T1 and T2 MRI at the end of the experiment for anatomical co-registration and brain ROI delineation	
[¹⁸ FJS and [¹⁸ FJ6	Development and test of new [¹⁸ F]fluorobenzene ring-based TSPO radiotracers	30-min intraluminal MCAO in male SD rats (7 weeks old, 220–240 g)	Nu	$[^{18}F]5: \text{ ipsi-'contralateral ration, } 4.49\pm0.26; \text{ BP}_{ND}, \\ 3.42\pm0.23 \\ \cdot [^{18}F]6: \text{ ipsi-'contralateral ration, } 2.98\pm0.37; \text{ BP}_{ND}, \\ 1.76\pm0.21 \\ \cdot \text{ Both have a better signal-to-noise ratio than that of } [^{11}C]+R-PK11195$		[75]
[¹⁸ F]DPA-714 [¹⁸ F]IAM6067 (S1R tracer) [92]	Comparison of in vivo PET with MALDI-MS imaging on long-term consequences of stroke on ND (S1R] and NI (TSPO)	Comparison of in vivo PET with 70-min distal left MCAO with CCAO MALDI-MS imaging on in male Wistar rats (350 g) long-term consequences of stroke on ND (S1R] and NI (TSPO)	3 months post-MCAO	ne in line and	T2 weighted (T2W) MRI at 48 h post-stroke confirmed the presence of infarct	[91]
[¹⁸ FJDAA1106	Automation of [¹⁸ F]DAA1106 synthesis	30-min intraluminal MCAO in male SD rats (7 weeks old, 220-240 g)	6-8 days post-MCAO	sphingomyelin in the ischemic scar • AUC _{20-60min} in the striatum: • Ipsilateral: 44.7±7.7 • Contralateral: 23.7±0.1 • Tipsi-/contralateral ratio: 1.9±0.3 • Pretreatment with unlabelled PK11195 (3 mg/kg)		[105]
[¹⁸ FJDPA-714	Examine longitudinal changes in TSPO after mild ischaemia with selective neuronal loss but without acute infarction	20-min intraluminal MCAO in male Wistar rats (9–10 weeks old, approx. 300 g)	• 2 and 7 days post-MCAO • ARG at day 1, 2, 3 and 7 post-MCAO	1.2 1.2 1.2 1.2 1.8±0.8; 0.2	• [18 F]DPA-714 in vitro ARG confirmed a significant increase in TSPO binding from day 1, increasing up to day 7 post-MCAO • Ibal and GFAP IHC confirmed the presence of activated microglia and astrogliosis.	[84]
[¹⁸ FJDPA-714	Evaluate the effects of BMSC administration on neuroinflammation after transient MCAO	90-min intraluminal MCAO in male F344/NSIc rats (250–270 g)	3 and 10 days post-MCAO	• BMSC administration does not decrease max. and mean SUV 3 days post-MCAO • Significant decrease in max. and mean SUV by BMSC administration at 7 days post-MCAO	• BMSC administration decreases infart volume • [184]DPA-714 in vitro ARG confirmed in vivo PET data • BMSC administration decreases the number of CD8α+T cells and CD68 microglia in the infarrt and nori; infarrt and access	[101]
[¹⁸ F]VUIIS1018A	Evaluation of new TSPO tracer [¹⁸ F]VUIIS1018A	30-min intraluminal MCAO in male SD rats (7 weeks old, 220-240 g)	7–9 days post-MCAO	• Ipsilateral 1 ¹⁸ FJVUIIS1018A uptake at 0.73 SUV vs contralateral uptake at 0.20 SUV at 60 min post-injection • Iost-contralateral ratio: 3.5	[¹⁸ F]VUIS1018A in vitro ARG and TSPO IHC confirmed in vivo PET data	[77]
[¹¹ CJDPA-713 [¹⁸ FJGE-180	Head-to-head comparisons of [11C]DPA-713 and [18F]GE-180	Permanent distal MCAO in 3-months-old female C57BL/6J mice	2, 6 and 28 days post-MCAO	se for ¹¹ C DPA-713 180 (1.10) DPA-713 and and 2.06, respectively)	• T2 MRI for ROI delineation • Ex vivo [¹¹ CJDPA-713 and [¹⁸ F]GE-180 ARG confirmed the PET data • CD68 and GFAP IHC confirmed the presence of activated microglia and astrogliosis in the infarct	[80] f

Table 3 (continued)						
PET tracer *	Rational	Stroke model and species	Imaging time points	Main imaging findings	Additional readouts	Ref.
[¹8F]FEPPA	Test the ability of TSPO to detect MHCII* microglia in WM post-stroke	Test the ability of TSPO to detect Intrastriatal injection of ET1 in male MHCII ⁺ microglia in WM Fischer 344 strain (11–14 months) post-stroke	Baseline and 7 and 28 days post-MCAO	maintained at 28 days (1.67 and 1.64, respectively) TSPO infarct/cerebellum ratio: • Baseline: 0.94±0.16 • Day 7: 2.10±0.78 • Day 28: 1.77±0.35 • Similar change in peri-infarct WM but not contralateral WM	L. Z.	[86]
[¹⁸ FJBR-351 (MMPs) [¹⁰ F]BR-351 (MMPs) [106] [^{99m} Tc]HMPAO (CBF)	Investigate NI through TSPO and 30-min intraluminal MMP PET imaging in stroke C57BL/6 mice (22–25 g)	30-min intrahuminal MCAO in male C57BL/6 mice (3-4 months old, 22-25 g)	24 to 48 h and 7±1, 14±1 and 21±1 days post-MCAO	• No increase in TSPO at 24–48 h • Significant increase at 7, 14 and 21 days, peaking at 14 days • Localization of increased [¹⁸ F]DPA–714 uptake is larger than T2w-MRI infarct, not the case for [¹⁸ F]BR-351 • Volumetric analysis: MMP expression peaks at 24–48 h and has a different spatio-temporal distribution than TSPO • MMPs increased at all time points, with an increase in the contralateral side at day 21	• Severity of stroke confirmed by [^{99m} Tc]HMPAO [95, and T2 MRI • TSPO and MMP9 IHC confirmed PET results	[95,
94] [¹ ⁸ F]CPFPX (A1AR) [107] [¹ ⁸ F]DPA-714 [¹ ⁸ F]FLT	Better understanding of the role of A1ARs on ischaemic damage	90-min intraluminal MCAO in male SD •[¹¹8F]CPFPX PET at rats (8 weeks old, 304±7.1 g baseline and 1, 3, 7, 14, 21 and 28 days post-MCAO • [¹¹8F]DPA-714 PET at 7 days post-MCAO		• Decrease in [¹8F]CPFPX uptake at day 1 returning to baseline level at day 3, gradually decreasing to reach significant differences vs baseline at days 21 and 28 post-WCAO • Treatment with A1AR agonist ENBA reduced [¹8F]DPA-714 uptake and [¹8F]FLT uptake infarct size and improved the neurological score	HC showed an increase in A1ARs at days 3 and 7 returning to baseline level 14 days post-MCAO localized on microglia and macrophages Treatment with A1AR agonist ENBA reduced CD11b/TSPO and Ki67 IHC staining in the infarct	[66]

*TSPO-PET tracers and associated results are in bold.

Abbreviations: l^{18} F/3, N-(4-[18F]fluorobenzyl)-N-methyl-2-(7-methyl-8-oxo-2-phenyl-7,8-dihydro-9H-purin-9-yl)acetamide; l^{18} F/36, 2-(5-(4-[18 F]fluorophenyl)-2-oxobenzo[d]oxazol-3(2H)-yl)-N-methyl-3(2H)-yl)-N-methyl-3(H)-yl)-N-methyl-3(H)-yl) methyl-N-phenylacetamide; [18 FJFDG, fluorodeoxyglucose; [18 FJFLT, fluorothymidine; [18 FJFSPG, (4S)-4-(3-18 F-fluoropropyl)-L-glutamate; [29 FJHMPAO, 99 TC-D,L-hexamethylenepropyleneamine oxime; AIAR, adenosine A1 receptors; ACA, anterior cerebral artery; ARG, autoradiography; BMSC, bone marrow stromal cell; CCAO, common carotid artery occlusion; CB2, cannabinoid type 2 receptors; CBF, cerebral blood flow; ET1, endothelin-1; IHC, immunohistochemistry; MALDI-MS, matrix-assisted laser desorption/ionization mass spectrometry; MCAO, middle cerebral artery occlusion; MHCII, major histocompatibility complex class II; MMPs, matrix metalloproteinases; nACIR, nicotinic acetylcholine receptor; ND, neurodegeneration; NI, neuroinflammation; NSC, neural stem cells; SIR, sigma-1 receptor; SAH, subarachnoid haemorrhage; SD, Sprague Dawley; SUVr, standard uptake value ratio; tDCS, transcranial direct current stimulation; TLR4, toll-like receptor; WM, white-matter; xc⁻, cystine-glutamate antiporter system



increase in uptake from day 3 post-MCAO was reported. peaking at day 7 and remaining elevated up to day 14 when compared to baseline [76], in line with previous reports [65]. The same observation can be made for [18F]F-DPA in terms of binding characteristics and uptake levels. However, its lower metabolism rate when compared to [18F]DPA-714 is an interesting feature of this new tracer [79]. Also performing a direct comparison between 2nd generation TSPO tracers. Chanev et al. [80] compared [11C]DPA-713 and [18F]GE-180 in a model of permanent MCAO in mice. In this study, they showed that, 1 day post-MCAO, [11C]DPA-713 uptake was significantly increased (+22%) whereas [18F]GE-180 uptake was not (+10%); 6 days post-MCAO, both tracers exhibited similar uptake increases (+120% and +106%, respectively) which remained elevated up to 28 days post-MCAO (+67% and +64%, respectively) [80].

The other major use of TSPO imaging in stroke models is to better understand the role of various neuroinflammation processes following experimental stroke. In that perspective, some studies used TSPO-PET imaging to better characterize the temporal and anatomical evolution of neuroinflammation in various models of experimental stroke, some of them new. De Lange et al. [81] used [18F]GE-180 to evaluate acute neuroinflammation in a model of hypoxia resuscitation in newborn piglets. Considering the numerous reports showing that it takes approximately 3 days for microglia to proliferate and TSPO expression to increase in stroke and LPS model of neuroinflammation, unsurprisingly this study did not detect any significant change in [18F]GE-180 between 5 and 32 h post-hypoxia. Similarly, in a model of subarachnoid haemorrhage (SAH) in rats, Thomas et al. [82] showed only a trend (p = 0.0519) in an increase in $[^{18}F]DPA-714$ uptake 2 days post-SAH. In a very clinically relevant model of focal temporary MCAO using a minimally invasive technique through the insertion of a microwire tip via the ventral tail artery, Toth et al. [83] demonstrated significant increases in [11C]PBR28 uptake in the infarct at day 4, 7 and 14 post-MCAO, although [¹¹C]PBR28 uptake started to decrease at day 14. Their results are in line with other studies using more conventional models of stroke in rats [76, 65] such as those developed by Miyajima et al. [84] described a significant increase in [18F]DPA-714 uptake in the infarct from day 2 maintained up to day 7 post-MCAO (20-min intraluminal MCAO). Taken altogether, these results confirmed that in these models of acute brain injury (permanent or temporary MCAO, SAH or hypoxia), the microglial/macrophage infiltration responsible for the TSPO increase takes approximately 3 days to become detectable, peaks about 1 week after injury and then slowly decreases in intensity afterwards.

On top of characterizing the temporal evolution of TSPO expression after stroke, some studies used TSPO-PET tracers combined with other PET tracers or other imaging methods to investigate further processes in stroke. Walter et al. combined

[11C]-R-PK11195 PET with USPIO MR imaging to differentiate nonphagocytic (TSPO⁺ only) vs phagocytic (TSPO⁺ & USPIO⁺) neuroinflammatory cells in a permanent microsphere-induced model of MCAO in rats 6-7, 26-27 and 55-56 days post-stroke [85]. Such combination of techniques allowed the authors to determine that brain regions with early phagocytic signal (USPIO⁺) at day 7 will irremediably evolve into necrotic tissue, whereas tissue exclusively positive for TSPO will remodel but remains viable thereafter (days 27 and 55 post-stroke). Looking at white matter damage after stroke, Al-Khishman et al. used [18F1FEPPA TSPO-PET imaging and reported a significant increase at 7 and 28 days in the striatal infarct and peri-infarct white matter (WM) [86]. In the contralateral WM, they were able to detect MHCII+ cells by either [18F]FEPPA TSPO-PET or TSPO IHC. In a way, this highlights the fact that TSPO is an imperfect surrogate marker of activated microglia and may be unable to detect certain phenotype of microglia.

Combining [11C]-R-PK11195 and [18F]FDG, Backes et al. [87] performed a study investigating the potential contribution of neuroinflammation to [18F]FDG signal in the same model as Walter et al. [85]. Not unexpectedly, they found that microglial activation and macrophage infiltration could indeed be the source of a significant [18F]FDG uptake at day 7 post-stroke in the peri-infarct region where [18F]FDG uptake was initially significantly decreased at day 1. These observations are in line with previous use of [18F]FDG to image inflammation [88–90], although very unspecifically especially in the brain where the basal [18F]FDG uptake is very high mostly due to neuronal activity. They concluded that in such brain regions, where metabolic supply was already decreased and likely insufficient, the contribution of neuroinflammation to the [18F]FDG signal might actually mask even more severe hypometabolism. Also looking at complementing PET imaging with another tracer and method, Henderson et al. [91] combined PET imaging with [18F]DPA-714 and the newly developed sigma-1 receptor (tracer [18F]IAM6067 [92] and post-mortem mass spectrometry imaging (MALDI-TOF) to look at the long-term consequences of distal MCAO. These authors did not find any changes in [18F]DPA-714 and [¹⁸F]IAM6067, suggesting that 3 months post-MCAO, neuroinflammation had resolved and that neuronal loss directly in or at a distance of the infarct was undetectable using S1R PET imaging. MALDI-TOF MS however revealed distinctive changes in the peri-infarct scar with a decrease in phosphatidylcholines, which are otherwise found in the healthy tissue, whereas sphingomyelin and lysophosphatidylcholine were significantly decreased in the same region. The MALDI-TOF MS combined with the TSPO-PET data suggest that neuroinflammation had fully recessed in the peri-infarct region 3 months after MCAO where scarification and repair were taking place. Using [11C]-R-PK11195 PET imaging as a reference for neuroinflammation imaging, Hosoya [93]



tested the potential of the cannabinoid type 2 receptor (CB2) as an early marker for neuroinflammation 24 h post-MCAO. They reported a significant increase in [11C]NE-40 uptake but no change in [11C]-R-PK11195 uptake. Further immunohistochemistry experiments revealed that most of the CB2⁺ cells were microglia (CD11B⁺) together with some neuron-glial antigen 2-positive (NG2⁺) cells putatively identified as monocytes, supporting CB2 and [11C]NE-40 as a potential candidate of early microglial activation, although in that case, the exact phenotype of the microglia remains to be established. Finally, investigating the relationship between microglial activation and metalloproteases (MMP), Zinnhardt et al. [94] and Barca et al. [95] investigated TSPO expression with [18F]DPA-714 and MMP levels with [18F]BR-351. These studies showed a differential temporal expression between TSPO and MMP; MMP levels increased early (days 1–7 post-MCAO) and remained elevated while TSPO levels increased later (days 7-21 post-MCAO) in the infarct. Interestingly, MMP were also significantly increased in the contralateral side at 21 days, where no change in TSPO could be detected. By refining the differential analysis of the two tracers and comparing it with the T₂-weighted MR map of the infarct, Barca et al. [95] concluded that this differential pattern likely represented a different phase of acute inflammation in the infarct followed by remodelling in the peri-infarct and contralateral side.

Focusing more on the rapeutic approaches in relation with neuroinflammation, Martin et al. published various papers using TSPO as reference for neuroinflammation imaging in which they examine the involvement of $\alpha 4\beta 2$ nicotinic acetylcholine receptor (nAChR) [96], the cystine-glutamate antiporter system xc⁻ [97], toll-like receptor 4 (TLR4) [98] and the adenosine A1 receptors (A1AR) [99] in the regulation of neuroinflammation after stroke. Overall, they described a very consistent time course of TSPO expression across studies and models. They also demonstrated that 2[18F]-fluoro-A85380 (α 4 β 2 nAChR) and [18 F]FSPG (system xc⁻) uptakes were maximum at 7 and 3-7 days post-stroke, respectively, and decreased thereafter, paralleling TSPO levels. Conversely, [18F]CPFPX (A1 adenosine receptor, A1AR) followed an inverse pattern to TSPO levels along time with an early decrease 24 h post-stroke returning to baseline at day 3 followed by a subsequent progressive decrease reaching significance vs baseline at days 21-28 post-MCAO. It must be noted that there was a slight discrepancy between the temporal expression of the A1AR measured by PET and immunohistochemistry as for the latter, there was no decrease observed at day 1 and no significant decrease at days 21-28 vs baseline. Altogether, these studies demonstrated that these systems are altered following stroke. More importantly, these studies also demonstrated that modulation of the $\alpha 4\beta 2$ nAChR by the selective antagonist DhβE increased [11C]-R-PK11195 uptake [96], whereas treatment with inhibitors of the system xc⁻ [97] or the A1AR agonist ENBA [99] significantly decreased neuroinflammation as measured by [18F]DPA-714 uptake and immunohistochemistry. In the same line, [11C]-R-PK11195 PET imaging showed that neuroinflammation was reduced in TLR4^{-/-} mice 2 days but not 7 days post-MCAO [98]. Similarly, Braun et al. [100] investigated the effect of transcranial direct current stimulation (tDCS) on neuroinflammation and neural stem cell (NSC) proliferation 16 days post-MCAO and showed no effect of tDCS on NSC proliferation as measured by [18F]FLT PET but did observe an effect when measured by immunohistochemistry; [11C]-R-PK11195 was unfortunately not quantified, and only a noticeable uptake in the peri-infarct and thalamus was reported. Finally, Tan et al. [101] evaluated the therapeutic effect of intravenous administration of bone marrow stromal cell (BMSC) to modulate the inflammatory response to stroke. They showed that [¹⁸F]DPA-714 uptake increased 3 days post-MCAO similarly in vehicle and BMSC-treated rats, but 7 days post-MCAO, [18F]DPA-714 uptake was significantly reduced in BMSCtreated animals compared to vehicle animals. The in vivo PET results and therapeutic effect of the BMSC treatment were confirmed by autoradiography and were correlated with a decrease in infarct volume as well as a decrease in the number of CD8α+ T cells and CD68 microglia in the infarct and peri-infarct areas.

Neuroinflammation in models of chronic neurodegenerative diseases

Alzheimer's disease (AD)

Similarly to stroke and other neurodegenerative diseases, neuroinflammation emerged as a potential essential player in the pathophysiology of AD in the 1990s [108, 109], although its presence was already acknowledged by Alois Alzheimer himself when he first described the neuropathological features of AD [110–112].

In 2019, Chaney et al. published a review of neuroinflammation imaging in Alzheimer diseases [113] that included preclinical references up to the work of Lopez-Picon et al. [114]. For this paragraph, we used the following PubMed search, "(omega* OR TSPO OR PBR OR PK11195) AND (PET OR positron) AND (brain OR cereb*) AND (Alzheimer) AND (rat OR mouse OR mice OR animal* OR experimental OR pig OR gerbil OR rabbit OR guinea OR model OR dog OR cat) AND (English[lang])", including all references since 2018; this search returned 37 records including 6 reviews. After exclusion of the reviews, clinical papers and non-PET imaging manuscripts returned by this search, 8 original research papers that included in vivo TSPO imaging were kept in this review and are summarized in Table 4.



 Table 4
 Overview of the preclinical TSPO-PET/SPECT imaging studies in Alzheimer's disease models (published since 2019 [113])

PET tracer *	Rational	AD model	Imaging time points	Main imaging findings	Additional readouts	Ref.
[¹⁸ F]GE180 [¹⁵ O]H ₂ O (CBF)	Investigate the short-term effects of space radiation (model by ⁵⁶ Fe irradiation at 4 months of age) on brain ageing and AD	3.5-months-old male and female APPswe/PS1d- E9 Tg mice	At baseline (3.5 month old) and 1.5–2 month post irradiation	• Irradiation induced a small decrease in the initial (0–20 min post-inj.) and late [¹⁸ F]GE180 uptake (20–60 min post-inj.) in Tg female mice only • No changes in any of the other groups • No change in CBF	 Irradiation induces a reduction in Aβ and CD68 IHC staining in Tg female only No effect on TSPO, Iba-1 or GFAP staining in any of the group 	[125]
[¹⁸ F]GE-180 [¹⁸ F]florbetaben (Aβ) [126, 127]	Establish serial small-animal PET as a tool for therapy monitoring of the new model of AD App ^{NL-G-F} mice	Males and females App ^{NL-G-F} knock-in [128] and WT mice	2.5, 5, 7.5 and 10 months of age	• Increased [18F]GE-180 SUVr in the cortex from 5 m and the hippocampus from 7.5 m in Tg mice, increasing further at 10m • Similar spatiotemporal pattern for an increase in [18F]florbetaben in Tg mice • Correlations between tracer uptake ([18F]GE-180 SUVr and [18F]GE-180/[18F]florbeta- ben ratio) and spatial learning performance in the right entorhinal/piriform cortex and the right amygdala (NS in left ROIs)	IHC for fibrillar and non-fibrillar Aβ and neuroinflammation markers (Iba1, TREM2) confirmed PET results	[116,
117]				,		
[¹²⁵ I]-CLINDE	Investigate the relationship between TSPO and Aβ load in AD mice	Female triple transgenic (3×TgAD, APP _{swe} , PS1 _{M146V} and Tau _{P301L}) and C57B1/6J-S- v129 control mice	21 months of age	 Increase [¹²⁵I]-CLINDE uptake in TG vs WT mice Significant spill over in the hippocampus from the nearby ventricular zones [¹²⁵I]-CLINDE uptake in the pituitary, lateral ventricles and cerebellum is specific (29.4±7.6 to 61±3.9% displacement by the unlabelled CLINDE) 	[125I]-CLINDE and [125I]DRM106 (Aβ) [129] ARG at 1, 6, 12 or 21 months confirmed in vivo SPECT result with [125I]-CLINDE and showed that TSPO increase precedes Aβ load in most of the hippocampal substructures	[124]
[¹¹ C]-R-PK11195 [¹¹ C]NE40 (CB2) [104]	Investigate microglial status in brain senescence	Male SAMP10 mice	5 and 15 weeks of age	• No change in [11C]-R-PK11195 at any ages • No change in [11C]NE40 SUVr at 5 weeks • [11C]NE40 SUVr > [11C]-R-PK11195 SUVr at 15 weeks	Increase in CB2/Iba1 ⁺ cells at 15 weeks suggesting an anti-inflammatory phenotype TSPO IHC consistent with low/basal level TSPO expression measured by	[123]
[¹⁸ F]FEPPA	Test the ability of TSPO to detect MHCII ⁺ microglia in WM in a rat model of AD	F344 and TgAPP21 rats	11–14 months of age	• No significant increase in [18F]FEPPA SUVr in previously reported [121] WM MHCII ⁺ microglia in TgAPP21 rats	PET	[122,
86] [¹⁸ F]DPA-714	In vivo assessment of neuroinflamma- tion in AD mice	B6.Cg-Tg (APP _{swe} , PSEN1 _{dE9}) 85Dbo/Mmjax and WT mice	6-7, 9–10, 12–13, and 15–16 months of age	 No TG vs WT differences at 6–7 and 9–10 months Increase in cortical (+40%) and hippocampal (+60%) 	IHC for Iba1 and TSPO confirmed and correlated with PET data	[120]



Table 4 (continued)

PET tracer *	Rational	AD model	Imaging time points	Main imaging findings	Additional readouts	Ref.
[¹⁸ F]F-DPA	Establish the impact of low molar activity tracer on specific brain uptake	Males and females TG APP/PS1-21 and WT mice	9 months of age	[18F]DPA-714 SUVr at 12-13 and 15–16 months • Significant increase in tracer SUVr in TG vs WT in more brain ROIs with high molar activity [18F]F-DPA • High molar activity tracer produced greater (1.5x) differences between TG and WT	ARG confirmed the TG vs WT differences in all brain ROIs Significant differences between low and high molar activity uptake in TG	[115]

^{*}TSPO-PET tracers and associated results are in bold.

Abbreviations: ARG, autoradiography; CBF, cerebral blood flow; CB2, cannabinoid type 2 receptor; IHC, immunohistochemistry; ND, neurodegeneration; NS, non-significant; ROI, region of interest; SAMP10, senescence-accelerated mouse prone 10; SUVr, standard uptake value ratio; system; TG, transgenic; WT, wild type

AD animal models need to be aged and are consequently expensive to breed and maintain. In such models and despite its cost, in vivo imaging presents the advantages of reducing the number of animals while increasing statistical power through a longitudinal (i.e. repeated) analysis of the same cohort of animals.

In a rather unusual study, Liu et al. used [¹⁸F]GE-180 PET to investigate the effect of space radiation on normal brain ageing and on AD between 3.5 and 5 months of age in mice. They found that irradiation had only a very limited effect on brain inflammation, with only a minute reduction in [¹⁸F]GE-180 uptake in female TG vs nonirradiated mice, no such effect was observed in male mice.

Keller et al. [115] reported the only paper that used the APP/PS1-21 model at 9 months of age to test a new TSPO ligand. In this paper, they wanted to evaluate the impact of low vs high molar activity of [18F]F-DPA on brain uptake. This is a relevant technical point to all preclinical PET studies. The molar activity of a tracer should not be neglected when performing PET imaging in small animals such as mice which have a small body weight and blood volume because the presence of a too high concentration of cold ligand (i.e. low molar activity) is more likely to impact the binding and may lead to a poor sensitivity of the measures to pathological changes. In this study, they reported a significant 1.5-fold difference in brain uptake in favour of the high molecular activity. However, it must be noted that in this article, the difference between the low and the high molar activity was particularly large (about 100-fold; 2.25±0.96 GBq/mmol vs 260±110 GBq/mmol), which is an extreme case scenario.

Most of the other studies reviewed here were trying to characterize and understand the temporal and anatomical pattern of neuroinflammation in various models of AD. Sacher et al. [116] and Biechele et al. [117] monitored neuroinflammation in the new App^{NL-G-F} model of AD in mice together with A β with [18 F]florbetaben. In this model, [18 F]GE-180 TSPO and A β levels started to increase at 5 months of age and continue to further increase up to 10 months of age, earlier than in other models such as the APP_{swe}×PS1 $_{\Delta$ E9 [118, 119], suggesting a rather aggressive AD-like phenotype. In agreement with these previous reports [118, 119], Hu et al. [120] reported no changes in [18 F]DPA-714 uptake in APP_{swe}×PS1 $_{\Delta$ E9 mice between 6 and 10 months of age with an increase in [18 F]DPA-714 SUVr becoming significant at 12 and 16 months of age.

Now trying to understand the meaning of TSPO signal or lack of it, Al-Khishman et al. [86] tried to determine the sensitivity of PET imaging to detect MHCII+ microglial cells as they did in a model of stroke (see above). Using the TgAPP21 transgenic rat model of AD and [¹⁸F]FEPPA PET, they showed no significant increase in [¹⁸F]FEPPA PET uptake in the TgAPP21 rats vs WT at 11–14 months of age, despite the same group demonstrating the presence of MHCII+ cells in previous reports [121, 122]. This observation confirms the one made in the stroke model [86] that TSPO-PET is not able or sensitive enough to detect all phenotypes of activated microglia.

Although related to AD, Yamagishi et al. [123] tried to address the slightly different question of the microglial status during brain senescence using a dual tracer study with [11C]-R-PK11195 for TSPO imaging and [11C]NE-40 for CB2 imaging in 5- and 15-weeks-old SAMP mice. In this study, the authors showed no TSPO expression at all ages but an increase in CB2 binding and expression at 15 weeks of age



compatible with an anti-inflammatory phenotype of the microglia.

Finally, and although the in vivo imaging performed by Tournier et al. [124] is restricted to only 1 time point (21 months old) in the 3×Tg mouse model of AD with [125] CLINDE, the authors interestingly showed a significant spill over signal in the hippocampus due to significant tracer uptake in the ventricles/choroid plexus. Interestingly, this observation highlights the difficulty to perform accurate quantitative in vivo imaging studies in mouse models of AD due to the small size of the mouse brain, also highlighting the importance of selecting fairly large ROIs (such as the whole cortex or whole hippocampus) to limit the impact of partial volume effects in mice brain imaging quantification. This is further illustrated by the fact that the dual autoradiography [125I]CLINDE/[125I]DRM106 (Aβ) allowed Tournier et al. [124] to demonstrate that increase in TSPO binding (from 6 months in the subiculum) preceded Aβ increase and that these increases affected various part of the hippocampus differentially (subiculum then antero-dorsal and dorsal hippocampus and finally ventral hippocampus).

Parkinson's disease

In 1988, McGeer and colleagues reported for the first time the presence of reactive microglia in the brains of Parkinson's disease (PD) patients [130]. They suggested what is now generally achieved that the immune system plays an active role and that neuroinflammation is not just a consequence of the ongoing neurodegeneration [131, 132]. Nevertheless, the interplay between cytokines, neurodegeneration, and protein aggregation as cause or consequence remains largely unknown today [133, 134, 131]. Over the last two decades, neuroinflammation in PD has been a strongly growing research area, but only few TSPO-PET studies [135-138] or TSPOautoradiography [139–141] studies have been reported in preclinical models. In addition, these studies generally report on the feasibility of monitoring brain inflammation but less on the mechanistic of neuroinflammation in PD. Recently, Belloli and colleagues [142] have provided a detailed overview of translational imaging studies in PD, including TSPO-PET imaging; complementary to this review, we only focus on TSPO-PET and autoradiography studies in preclinical models of PD. We used the following search in PubMed, "(omega* OR TSPO OR PBR OR PK11195) AND (PET OR positron) AND (brain OR cereb*) AND (Parkinson OR Parkinson's disease OR synuclein) AND (rat OR mouse OR mice OR animal* OR experimental OR pig OR gerbil OR rabbit OR guinea OR primate OR dog OR cat) AND (English[lang])", which returned initially 16 records, of which only 6 references referred to TSPO-PET imaging studies in preclinical models. An overview of TSPO-PET in preclinical PD models is shown in Table 5.

One of the most gold standard models of PD consists of the intracerebral injection of 6-hydoxydopamine (6-OHDA) – in the substantia nigra (SN), medial forebrain bundle (mfb), or striatum (STR) – which leads to dose-dependent progressive neurodegeneration and transient neuroinflammation [140, 141, 143, 144]. Cichetti et al. described the time course of tyrosine hydroxylase (TH⁺) cell loss in parallel to microglial activation up to 30 days post-striatal lesion (24µg) and demonstrated dramatic increase in TSPO signal in ventral mesencephalon and striatum 21 days after 6-OHDA lesioning using [11C]-R-PK11195 [144]. Maia et al. further developed this work by measuring the time course of the neuroinflammatory response in STR and SN using in vitro binding of [3H]-R-PK11195 and ex vivo uptake of [123] CLINDE, in parallel to changes in dopamine transporter (DAT) binding and TH⁺ protein levels after 6-OHDA-induced striatal lesion (10 µg) [140]. The TSPO binding in STR peaked 7 days post 6-OHDA induction and then declined progressively at 4 weeks, until disappearing at 8 weeks post-injection. In the SN, a delayed but similar response was observed with maximal TSPO binding at 14 days post-injection. The neuroinflammatory response as measured with TSPO ligands occurred concomitantly with a progressive loss in TH⁺ cells and DAT; however, in this study, it was not identified which glial cell type was TSPO positive. Noteworthy, the same group [141] recently draw a complete metabolomics, neurodegenerative and neuroinflammatory picture of a new variation of the 6-OHDA model (triple striatal injection, 12 µg) through the combination of multiple techniques, amongst which autoradiography using [3H]FPA714. In the search for new radioligands more specific for the microglial response, Crabbé and colleagues used the acute transient neuroinflammation of the 6-OHDA model (striatal induction, 24 µg) to compare a new microglial-specific PET ligand targeting the P2YX7 receptor, [11C]JNJ717, with the well-validated TSPO ligand [18F]DPA-714 [139]. Their TSPO autoradiography study revealed a comparable striatal and nigral TSPO binding pattern as initially described by Maia and colleagues [140]. Surprisingly, the binding of the microglial-specific ligand showed a different temporal pattern than the one observed with the TSPO ligand [18F]DPA714 [139]. In the striatum, the microglial response was detectable at 7 days, but maximal around 14 days post-injection, in contrast to the TSPO response which was maximal at 7 days. In the SN, an acute microglial response was observed at 7 days, which was observed until 28 days after injection with TSPO-PET ligand [139]. In a 6-OHDA mouse model (2 µl of 5 mg/kg in the SN), Fricke et al. transduced cells in the subventricular zone with a lentivirus encoding for firefly luciferase to follow the migration of progenitor as a response to neurodegeneration induced neuroinflammation, which was imaged with [¹⁸F]DPA714 [145]. Finally, Nomura et al. showed that LPS-induced peripheral inflammation exacerbated the



 Table 5
 Overview of the preclinical TSPO-PET/SPECT imaging and autoradiography studies in Parkinson's disease models

PET tracer	Rational	Parkinson model			Imaging time	Major outcomes	Ref.
		Toxin	Dose	Species	points		
[¹¹ CJ-R-PK11195 [¹¹ CJ-R-PK11195	Associate the neuroinflammatory response to 6-OHDA-induced dopaminergic cell loss	6-ОНDА	20–24 µg/striatum	Rat	21 days post-injection	Progressive TH ⁺ cell loss in STR and SN paralleled with microglial activation; this coincided with positive TSPO-PET signal in SN and STR 3 weeks post-striatal lesion	[144,
[¹⁸ F]DPA-714	Compare a new microglial-specific ligand targeting P2X7 with a well validated TSPO-ligand in an acute (and chronic) PD model	6-ОНДА	24 µg/striatum	Rat	4–28 days post-injection	In the 6-OHDA model, maximal TSPO signal was observed in the STR 7 days, and in SN 14 days post-lesion. Uptake decreased until it disappeared in STR 28 day post-injection but	[139]
[¹²⁵]]CLINDE, [³ H]-R-P- K11105	Longitudinal monitoring of 6-OHDA-induced neuroinflammation and neurodegeneration	6-ОНДА	10 µg/striatum	Rat	3–56 days post-injection	Maximal TSPO signal in the STR 7 days and in SN 14 days post-lesion, then declining until it disputes 8 weeks week injection	[140]
[¹⁸ F]DPA-714	Evaluate with bioluminescence the migration of progenitor cells in a response to neurodegeneration-induced neuroinflammation, monitored with in vivo PET imaging	6-ОНDА	2 µl of 5 mg/kg	Mice	7, 14, 21 days post-injection	disappears of weeks post-injection 6-OHDA-induced neuroinflammation-associated neuroinflammation, both detectable by PET imaging. However, this did not result in any migration from the subventricular zone	[145]
[¹¹ C]-R-PK11195	Characterize the distribution of TSPO bindings sites in the brain and evaluate the feasibility of [¹¹ C]-R-PK11195 to monitor this binding in healthy, MPTP-treated, and MPTP+grafted brain	MPTP	Not specified	Landrace pigs and Götting- en minipi-	Baseline and 2 weeks after MPTP and 3 months after grafting	Despite a high expression of TSPO-binding sites in the porcine brain, ['IC]-R-PK11195 has a too low specificity in vivo	[147]
[¹¹ C]- R-PK 11195 [¹⁸ F]FEPPA	^{[11} C]-R-PK11195 Monitor early dopaminergic changes and ^{[18} F]FEPPA early glial response in a low-dose MPTP model	MPTP	Chronic intoxication 0.1/0.2, 0.6/0.8 mg/kg (IV, IM)	ss NHP	At baseline and during intoxication	TSPO-PET coincides with a decrease in striatal VMAT2; earlier and robust TSPO-PET signals result in earlier and more severe parkinsonism	[138,
¹¹ CJ-R-PK11195	[¹¹ C]-R-PK11195 Evaluate the role of TREM2 in the regulation of microglia to acute neurotoxic response	MPTP	4x 20 mg/kg (IP)	Mouse (TREM2 ^{-/-} vs WT)	1–7 days post-injection	TSPO-PET signal gradually increased in STR and SN, reaching significance in STR 2 days after intoxication; TREM2 ^{-/-} mice showed an earlier increment of [¹¹ C]-R-PK11195 binding	[149]
[¹¹ C] PBR28	Evaluate the impact of an acute peripheral inflammatory response on the progression of Parkinson's disease	LPS	Systemic	Rat $(LRRK2 p G2019S vs WT)$	10 months post-injection	and a significant increase of 11.74 Systemic LPS treatment caused inflammation in [22] the brain, detectable with TSPO-PET. LPS-treated LRRK2 animals exhibited significantly increased neuroinflammation in the cortex and ventral regions compared to	[22]
[¹ ⁸ F]FE PPA	Evaluate the capability of [¹⁸ F]FEPPA to detect a neuroinflammatory response in a	6ОНDA LPS	30 µg/striatum (unilateral)	Rat	2 days post-injection	control animals Systemic inflammation induced after 6OHDA-induced neuroinflammation results	[146]



_
\sim
.0
ത
\simeq
\sim
_
.=
7
Ĭ
=
0
$-\bar{c}$
· •
S
e
_
9
able

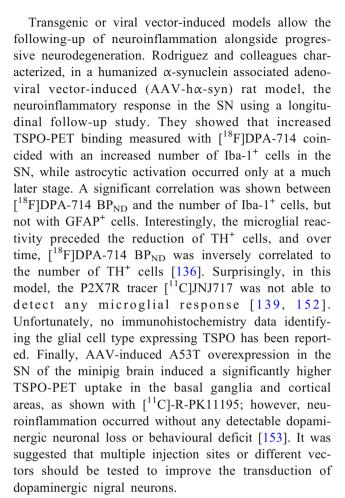
,							
PET tracer	Rational	Parkinson model			Imaging time	Major outcomes	Ref.
		Toxin	Dose	Species	pontes		
	PD model of primary neurotoxic microglial activation		Systemic		4 h post-injection	in higher expression of the pro-inflammatory cytokines IL- 1β and TNF- α ipsilateral to the lesion, which correlates with higher TSPO-PET signal in the lesion, as detected with 1^{18} FIFEPPA	
[¹¹ C]-R-PK11195	[¹¹ C]-R-PK11195 Validation of prostaglandin 2 (PGJ2) infusion in the SN as a PD model of chronic inflammation	PGJ2	16.7 µg/SN	Mouse	7 days post-injection	Chronic PG/IZ administration induces slow-onset [155] PD-like pathology with localized neuroinflammatory response localized in the SN	[155]
[¹⁸ FJDPA-714	Characterization of neuroinflammatory response in a rat model of progressive dopaminergic degeneration	AAV-hα-syn	8 × 10 ¹² gcp/mL/S- Npc (bilateral)	Rat	1, 3 days post-injection; 1–3, 16 WPI	Increased TSPO-PET binding coincided with an increased number of Iba-1 ⁺ cells in the SN, but astrocytic activation occurred only at a much later stage; significant positive correlation between BP _{ND} and the number of Iba-1 ⁺ cells, but not with GFAP ⁺ cells, inverse correlation between BP _{ND} and the number of TH ⁺ cells; microglial reactivity preceded the reduction of TH ⁺ cells.	[136]
[¹⁸ FJDPA-714	Compare a new microglial-specific ligand, targeting P2X7, with a well validated TSPO-ligand (in an acute and) chronic PD model	AAV-[A53T]-α-syn	9 × 10 ¹¹ gcp/mL/S- Npc (unilateral)	Rat	28, 42 days post-injection	Increased TSPO binding in SN between 28 and 42 days and 63 days in the STR; the same model imaged with the microglial PET ligand did not reveal any significant microglial activation; histological data to show the origin of TSPO-PET data are not available	[152,
[¹¹ C]-R-PK11195	[11C]-R-PK11195 Multitracer PET imaging study to characterize proteasome inhibitor induced model	Lactacystin ICV	200-400 µg	Minipig	Up to 6 months post administration	Lactacystin leads to the presence of mild neuroinflammation detectable with [¹¹ C]-R-PK11195; in addition, PET imaging revealed early deficits in the dopaminergic, serotonergic and noradrenergic systems, consistent with Break staring.	[151]
[¹¹ C]-R-PK11195	Characterization of microglial and dopaminergic response to overexpression of α-syn in the minipig brain	AAV-[A53T]-α-syn 1.04x 10 ¹⁴ to 1.16x10 ¹⁴ gcp/mL/SN (unilateral)	1.04x 10 ¹⁴ to 1.16x10 ¹⁴ gcp/mL/SNpc (unilateral)	Minipig	4 months post-injection	V _T was significantly increased in basal ganglia and cortical regions, in the absence of any motor symptoms or dopaminergic neuronal loss as revealed with in vivo PET or post-mortem studies	[153]



neuroinflammatory response to 6-OHDA. 6-OHDA lesioned animals treated with LPS showed higher expressions of proinflammatory cytokines at the site of the lesion, which was correlated with an increased TSPO-PET signal [146]. In conclusion, the 6-OHDA induces neuroinflammation-associated neurodegeneration, even though the neuroinflammatory reaction should rather be considered as acute, which is not representative of the slow chronic evolution of PD.

The lipophilic compound 1-methyl-4-phenyl-1,2,3,6tetrahydropyridine (MPTP), after crossing the blood-brain barrier, is metabolized by astrocytes. The metabolite, MPP+, is transported into dopaminergic neurons through the DAT where it accumulates and causes toxicity through binding at the mitochondrial complex I. The first PET imaging study on this model was performed on the porcine brain by Cumming et al. who first identified the cerebral distribution and saturation parameters of TSPO binding sites (at that time still referred to as PBBS) by a quantitative [3H]PK1195 binding study. Subsequent in vivo *PET* imaging with [11C]-R-PK11195 was not successful in Landrace pigs despite the high presence of TSPO-binding sites; in Göttingen minipigs, a displaceable signal was detected, which tended to increase 2 weeks after MPTP treatment. Overall, they concluded that [11C]-R-PK11195 has a too low specificity to detect TSPObinding sites in the porcine brain [147]. Chen et al. evaluated in the NHP, the time course of dopaminergic neuronal changes and neuroinflammation after chronic MPTP intoxication. In this parkinsonian model, they reported a transient increase in TSPO-PET uptake, measured by [11C]-R-PK11195, which coincided with a decrease in striatal vesicular monoamine transporter type 2 (VMAT2) binding before any decrease in DAT binding was observed [138]. Another study, also in the NHP MPTP model, reported on the neuroinflammatory response in relation to gender, neuroinflammatory cytokines and gut microbiota. It was shown that early and robust [18F]FEPPA PET signals coincided with earlier and more severe parkinsonism, which were especially seen in male compared to female NHP [148]. MPTP-induced neuroinflammation has further been applied in TREM2-deficient mice, using [11C]-R-PK11195, to demonstrate a central role of TREM2 in the regulation of microglial response to acute neurotoxic insults. Additionally, these data suggested a potential modulatory role of TSPO in response to immune system deficit [149].

Proteasomal inhibitors, such as lactacystin, cause dose-dependent dopaminergic neurodegeneration and are an alternative approach to model PD. In this context, a recently developed minipig parkinsonian model [150] has been evaluated in a multitracer PET study to investigate the longitudinal effect of chronic intracerebroventricular (ICV) exposure on monoaminergic projections and neuroinflammation, as evaluated with [11C]-PK11195 [151]. The results of this promising study showed that this model might better reflect early mechanisms in Parkinson's disease pathology.



Finally, the role of LRRK2 in the immune system underlies one of many hypotheses why LRRK2 p.GS20195S mutation is one of the most common risk factors for PD. As peripheral administered LPS induces a neuroinflammatory response that eventually can lead to specific loss of dopaminergic neurons [15], LPS is an appealing tool to assess the association of peripheral-induced neuroinflammation in the progression of PD. In this context, a longitudinal [11C]PBR28 TSPO-PET study was performed on rats carrying the LRRK2 p.GS20195S mutation and non-transgenic littermates treated peripherally with LPS (3mg/kg, i.p.) or vehicle. This study revealed a significant increased TSPO-PET signal in transgenic rats 10 months after systemic LPS challenge compared to saline-treated non-transgenic littermates [22]. Interestingly, these authors calculated age-centred SUV by subtracting the mean SUV of all saline-treated animals from each individual rat's SUV to account for the effect of age on neuroinflammation. This was based on previous work of the same group [154], where they reported on the sensibility of [11C]PBR28 TSPO-PET to ageing, which might be related to increased microglial activity in the ageing brain. In addition, in this study, the authors validated that the SUV measure is highly correlated with and less variable than the V_T quantification parameter.



Huntington disease

Huntington's disease (HD) is caused by a polymorphic trinucleotide CAG repeat expansion in the HTT gene that encodes the polyglutamine (polyQ) repeat in the N-terminal region of Huntingtin (Htt). These expansion repeats induce neuropathological hallmarks including a substantial accumulation of the Htt aggregates in the cortex and striatum [156]. These Htt-aggregated fragments set in motion a complicated cascade of both damaging, compensatory molecular processes and neuroinflammation, which is an important early pathological process of the disease. Activated microglia have been detected in brains from presymptomatic HD carriers [157] to postmortem HD patients [158] together with elevated inflammatory cytokines in both the CNS and plasma from HD patients [159].

Finding from animal models have an important contribution to elucidate pathways that are disrupted and have provided insights into the pathogenesis of this disease, enabling the development of therapeutic strategies [160]. As no spontaneous occurring animal models of HD exists, this pathology is modelled by toxins and viral vectors or through the use of transgenic animals.

The administration of either excitotoxic agents – such as quinolinic acid (QA) - or mitochondrial toxins, such as 3nitropropionic acid (3NP), can replicate some elements of the disease in both rodents [161, 162] and non-human primates (NHP) [163–165]. QA is an endogenous NMDA receptor agonist with excitotoxic properties. The excessive activation of NMDA receptors leads to a massive increase of calcium influx in neurons that involves the production and release of free radicals (reactive oxygen and nitrogen species), which can trigger cell oxidative damage leading to neuronal death. This model has been characterized by severe and fast (within 48 h) neuronal degeneration (GABAergic medium spiny neurons) as shown by the loss of NeuN staining [166]. Factors released during this degenerative process rapidly induce a proinflammatory environment leading to the activation of surrounding microglial cells and astrocytes [167]. Intracerebral injection of QA results in a reproducible lesion that -when injected in the striatum – reproduces some biochemical, behavioural and pathologic features of HD in rodents and nonhuman primates [168, 169, 167, 164]. In the 3NP (3nitropropionic acid) model, Ramachandran et al. [170] have reported increased mRNA expression of pro-inflammatory markers and of GFAP compared to controls 14 days after toxin administration.

TSPO-PET imaging in HD models has mainly been reported in the QA excitotoxic model since the localized, transient neuroinflammatory lesion facilitates the short-, to mid- and to long-term evaluation of TSPO-PET/SPECT radiotracers. A summary of the TSPO-PET imaging studies in HD is provided in Table 6. In all TSPO-PET/SPECT imaging studies

reported, OA was unilaterally injected in the striatum, using the contralateral side as an internal control. All excitotoxic QA models were induced in rodents, except for one study that reported TSPO imaging of [18F]-DPA-714 in non-human primates [171]. As such, the OA model has been used either to characterize the properties of new TSPO-PET/SPECT radiotracers ([125]]CLINDE [168, 172], [18F]DPA-714 [171], [3H]-PK11195 [173]) or to evaluate therapeutics or TSPO ligands as neuroprotective agents [174, 175]. Furthermore, short- to long-term NI changes post QA lesion were explored in transversal and longitudinal TSPO-PET imaging studies to correlate TSPO expression with glial reactivity in this model [172, 171, 176]. Overall, these studies reported a concomitant increase in TSPO radiotracer binding together with an increase in IHC inflammatory markers in the lesion. Arlicot et al. evaluated the properties of the [125I]CLINDE tracer at 6 days post QA injected at different doses [168]: microglial activation in the ipsilateral striatum was clearly observed using immunohistochemical (IHC) staining (OX-42 antibody), and authors evidenced a positive relationship between the intensity of IHC OX-42 staining and the dose of injected QA. Longitudinal TSPO-PET studies up to several months post-injection have also compared the time course of neuroinflammation with neurodegeneration, evaluating additionally the relative contribution of activated microglia and activated astrocytes in TSPO overexpression. Overall, longitudinal studies described a temporal transitory neuronal loss and reactive gliosis in the lesioned striatum. In Arlicot et al., TSPO expression was elevated from day 4 to 30 after QA administration with a maximal [125] CLINDE binding at 4, 7 and 14 days post-injection followed by a decline from day 30 down to day 90 [172]. In Lavisse et al., the level of TSPO immunoreactivity markedly increased from day 7 and was maximal between day 21 and day 40 and then decreased in intensity until day 91 [171]. The [¹⁸F]-DPA-714 total distribution volume increased initially in the restricted centre of the injection site from day 7 and progressively encompassed a larger area from day 7 to day 21 and remained visible on day 49. The same spreading observation was reported by Moresco et al. with a parallel increase of [11C]-R-PK11195 binding and microglial activation (and macrophage infiltration) markers as revealed by OX-42 staining, in both striatal and extrastriatal areas. These increases were maximum 7 days after QA injection, but OX-42 staining disappeared at later time points (30 and 60 days) while [11C]-R-PK11195 binding was still increased although in the restricted lesioned area. This observation led to hypothesize the presence of reactive astrocytes as [11C]-R-PK11195 presumably binds also to this cell type [177].

In some of these longitudinal studies, the astroglial and microglial activation, in parallel to neuronal loss, was characterized at several time points from 1 to 60–90 days post-QA injection, by double or triple immunostaining with GFAP, OX-42, Iba1 or CD68 and TSPO antibody. Moresco et al.



Table 6 Overview of the preclinical TSPO-PET/SPECT imaging studies in Huntington's disease models

PET/SPECT tracer	Rational	HD model and species	Imaging time points	Main imaging findings	Additional readouts	Ref.
[¹²⁵ I]CLINDE	Characterization and validation of the tracer at different stages of excitotoxic lesion	QA (*); 75, 150, 300 nmol in male Wistar rats	6 days post injection	Specificity confirmed with PK1195 blocking studies (-82% decrease). Significant [125 I]CLINDE uptake increase in lesioned compared to intact side	Autoradiographic analysis (including blocking) and IHC confirmed in vivo results	[168]
[¹²⁵ I]CLINDE	Investigation of the spatial and temporal density of TSPO after excitotoxic lesion	QA (*) 150 nmol in male Wistar rats	1, 7, 14, 60, and 90 days post injection	 Uptake sign increased in the lesioned striatum from 1 to 60 days Uptake increase until day 4 and plateau at 4–30 days. Progressive decrease at 30–90 days 	Autoradiography of TSPO expression corresponded to the temporal profile of both microglial activation and astrogliosis. Maximal astrocytic response at 7–14 days and at 14 days for microglia	[172]
[¹¹ C]-R-PK11195	Combination of in vivo, ex vivo and IHC approaches to analyse both short- and long-term changes in the QA model	QA (*) 210 nmol in Wistar rats	8, 30 and 60 days post injection 30 and 60 days post injection	At 8, 30 and 60 days, [11C]-R-PK11195 binding values are found to be 3.4, 3.0 and 2.8 times higher than those of the control	Reduction of both A2A and dopamine D2 receptors together with an augmentation of microglial activation/macrophage infiltration both in the lesioned striatum and, to some degree, also in extrastriatal areas	[176]
[¹⁸ F]DPA-714	Pharmacological Characterization of the tracer and evaluation of the cellular contribution to the PET signal	QA (*) 180 nmol in cynomol- gus NHP	7, 21, 40 90 days post injection	 VT: +17%, +54%, +157% and +39% higher than baseline on days 7, 14, 21 and 91. Decrease of uptake (-73%) in the lesioned striatum after blockage with PK11195 	IHC demonstrated progressive microglial activation from day 2 followed by delayed astrocytic reaction reaching maximum between 7 and 14 days. High correlation with in vivo results (r^2 =0.98)	[171]
[¹⁸ F]PBR06	Evaluation of the feasibility to detect activated microglia in these models	R6/2 , BACHD transgenic mice	Early, mid- and advanced stages	In R6/2 mice (advanced stage): • [18F]PBR06 accumulation in each ROI significantly higher by 25–30% compared with WTs • Reduction of 39–45% of uptake after blocking with PK11195 • Elevated [18F]PBR06 uptake in BACHD mice (early stage) compared with WTs in each ROI	TSPO expression correlated to microglial activation (increased IBA-1) and increased striatal levels of pro-inflammatory cytokines (IL-6 and TNFa)	[187]

used complementary autoradiography and confocal laser-scanning microscopy techniques to explore striatal and extrastriatal changes after QA injection with a finer analysis of cellular and subcellular events triggered by QA injection [176]. The time course of [125]-CLINDE binding matched with the temporal profile of both microglial and astrocyte reaction in Arlicot et al. study [172]: increased staining of GFAP-immunoreactive astrocytes was maximal at days 7 and 14 while microglial IHC marker peaked at day 14. They both then significantly decreased at days 60 and 90. Since [125]-CLINDE binding followed the same temporal profile

and co-localized in autoradiographic slices, authors concluded that both reactive astrocytes and microglia contributed to TSPO expression and signal. These observations were not in agreement with the results observed by Ryu and colleagues who reported that TSPO was primarily expressed in immunoreactive microglia and weakly in GFAP immunoreactive astrocytes, 24 h after QA injection [175]. This discrepancy could be partly explained by the different dose of injected QA used in these two studies (150 and 60 nmol in Arlicot et al. and Ryu et al., respectively) and the early time of imaging as astrogliosis has been reported to occur at later stages after



lesion. Moreover, intrastriatal OA lesion in the NHP has shown to induce progressive microglial activation from day 2 (Iba-1 labelling) with a delayed astrocytic reaction reaching maximal expression at 7 and 14 days [171]. The activated microglia were detected in the core of the lesion area whereas cell bodies of reactive astrocytes were organized as a perilesional rim with long and straight processes entering the lesion core from the periphery, as previously reported in rats [178]. Triple immunostaining studies (TSPO, GFAP and CD68 antibodies) provided further evidence that the [18F]DPA-714 PET signal primarily originated from activated microglia in this model (TSPO and CD68 staining colocalization) although it had previously been noted that this TSPO radiotracer binds to reactive astrocytes in a model of selective astrocytes reactivity [179]. Indeed, reactive astrocytes are known to be molecularly and functionally heterogeneous and their molecular profile can depend on the induceddisease context, the disease stage or the considered brain region [180].

Neurotoxin models were developed before the discovery of the Htt genetic mutation. The identification of the genetic mutation in HD led to the generation of a variety of animal models that express different forms of mutant huntingtin (expression of either full-length or N-terminal fragments of mutant Htt) showing different pathological spectra of the disease [181]. For example, the R6/2 mouse model carrying an N-terminal exon 1 fragment of the disease-causing human HTT gene displays physiological and behavioural phenotypes including progressive weight loss, shortened life span, progressive motor dysfunction and cognitive decline [182, 183]. A wide range of gene dysregulations has been reported in various brain regions of R6/ 2 mice including the expression of multiple inflammation- and stress-related genes as well as genes related to neurodegeneration [184]. In the brain of the R6/2 mouse model, significantly elevated pro-inflammatory cytokines were detected such as interleukin 6 (IL-6) and tumour necrosis factor alpha (TNF α) [185]. At early disease stages, microglia have been shown to be abnormal through ferritin accumulation and Iba1 immunostaining, and these abnormalities correlated with disease severity [186]. However, to the best of our knowledge, only one TSPO imaging study in transgenic models has been reported yet. In two HD mouse models, Simmons et al. assessed the feasibility of utilizing TSPO-PET imaging with the [18F]-PBR06 ligand to detect activated gliosis [187]. [18F]-PBR06 revealed microglial activation at a late disease stage in R6/2 mice, and at early to mid-stage in symptomatic BACHD mice. The [18F]-PBR06 TSPO-PET signal was correlated with increased Iba-1 and TSPO IHC staining in both models, and correlation was particularly strong in the striatum, cortex and hippocampus while GFAP levels did not correlate with [¹⁸F]-PBR06 uptake. These results indicated that TSPO seems to be predominately expressed on activated microglia in the brain in these transgenic models.

(*), unilaterally injected in the striatum; *IHC*, immunohistochemistry; *WT*, wild type

Models of multiple sclerosis

The PubMed search used for this paragraph was "(omega* OR TSPO OR PBR OR PK11195) AND (PET OR positron) AND (brain OR cereb*) AND (multiple AND sclerosis) AND (rat OR mouse OR mice OR animal* OR experimental OR pig OR gerbil OR rabbit OR guinea OR model OR dog OR cat) AND (English[lang])"; it returned 54 references, including 23 reviews; once Molecular Imaging and Contrast Agent Database entries, clinical studies and reviews were excluded, 11 preclinical studies were kept for this review. All these studies are summarized in Table 7.

Various studies investigated the neuroinflammatory profile of different models of MS (EAE or WM lesion) using [¹⁸F]PBR111 [188], [¹⁸F]VC701 [189], [¹⁸F]GE-180 [190–192] or [18F]DPA-714 [193, 194] PET tracers. Overall, TSPO imaging studies in MS models consistently reported a moderate to large increase in TSPO tracer uptake in the affected brain regions. Using an interesting model of relapsing experimental autoimmune encephalomyelitis (EAE) in mice, Mattner et al. [188] demonstrated a high increase (+135%) in [18F]PBR111 uptake during the 1st episode before the signal returned to baseline during the 2nd episode and bounced back up during the 3rd episode, demonstrating the interest of using TSPO imaging to monitor different stages of the disease in the preclinical model but with also important implication for translational application. The in vivo PET data were confirmed by IHC, demonstrating that TSPO expression was limited to microglial cells while astrocytes were TSPO negative. Additionally, Nack et al. [190] reported that TSPO⁺ cells were microglia following cuprizone treatment and that supplementing Cuprizone with MOG₃₅₋₅₅ peptide immunization drove the recruitment of TSPO⁺ monocytes in the lesion contributing to the overall PET signal on top of resident activated microglia; these results are in agreement with a more recent study with [18F]DPA714 [194]. Interestingly, Zinnhardt et al. [193] showed using [18F]DPA714 that during demyelination TSPO⁺ cells consisted only of microglia, while during remyelination, astrocytes also became TSPO+. Using [11C]-R-PK11195 TSPO-PET as a potential readout for therapeutic intervention, Converse et al. [195] aimed to evaluate the response to minocycline, an antibiotic that also represses microglial activation, in the zymosan-induced WM lesion in rats. They demonstrated an increase in [11C]-R-PK11195 uptake in the WM lesion that was significantly reduced by minocycline. More recently, Vainio et al. [191] investigated the response to an anti-VLA4 (very late antigen-4 integrin) antibody treatment in an EAE model in rats and demonstrated only a trend to increase in [18F]GE-180 uptake following 2 weeks of treatment but interestingly a rebound in



 Table 7
 Overview of the preclinical TSPO imaging studies in models of multiple sclerosis

PET tracer *	Rational	MS model and species	Imaging time points	Main imaging findings	Additional readouts	Ref.
[¹¹ C]-R-PK11195	Advance in vivo imaging methodology for studying microglial activation and therapeutic response to minocycline after WM lesion	Zymosan A stereotaxic injection in the CC of female SD rats (250±19g)	7 days post-injection	Increased [11C]-R-PK11195 uptake in the zymosan-injected WM 46% reduction in [11C]-R-PK11195 uptake in the minocycline-treated group	[³ H]-R-PK11195 ARG confirmed the presence of NI in the zymosan-injected WM	[195]
[¹⁸ F]PBR111	Investigate NI at different phases of EAE	Subcutaneous injection of PLP ₁₃₉₋₁₅₁ peptide in female SJL/J mice	Baseline and 6, 13, 20, 27, 35 and 41 days post immunization	• Peak increase (+135 ±20%) in [¹⁸ F]PBR111 uptake in all brain ROIs after the 1st episode • Return to baseline during the 2nd episode • Significant increase during the 3rd episode	IHC for TSPO and F4/80 and CD11b confirmed the increase in TSPO expression observed by PET to be microglial, GFAP+ cells were negative for TSPO	[188]
[11C]-R-PK11195 [11C]MeDAS (myelin) [200] [18F]FDG	Assess the feasibility of in vivo monitoring of MS-specific disease processes with PET	Demyelination by stereotactic injection of 1% lysolecithin in the CC and striatum of male SD rats (8–10 weeks old)	[18F]FDG and [11C]-R-PK11195 imaging at 3 days and 1 and 4 weeks and [11C]MeDAS PET at 1 and 4 weeks after injection	No change in [18F]FDG uptake +84% and +37% in [11C]-R-PK11195 SUV in the lesion and ipsilateral hemisphere at 3 days and 1 week, returning	Iba1 IHC confirmed the increase in NI in the CC and striatum 3 days and 1 week post-injection I¹¹C]MeDAS ARG showed a 57% decrease in myelin binding in ipsilateral CC Myelin IHC confirmed demyelination at 3 days and 1 week and partial remyelination at 4 weeks	[198]
[11C]-R-PK11195 [18F]FDG [18F]FSPG (system xc') [103]	Better understanding of system xc ⁻ in NI in MS	Subcutaneous injection of MBP in male Lewis rats (8 weeks old, 200–220 g)	Baseline and at 7, 14, 21 and 28 days after EAE induction	in FDG • Significant increase in [11C]-R-PK11195 uptake in the cerebellum and cervical and lumbar spinal cord at 14 days • Significant increase in [18F]FSPG uptake in the lumbar spinal cord at 14 days, normalized by administration of liposome-encapsulated	 Liposome-encapsulated clodronate treatment tends to worsen neurological score but reduced IHC Iba1 staining Suggest that microglia are the source of system xc⁻ in NI 	[199]
[¹⁸ F]VC701	Evaluate NI in a mouse EAE using TSPO-PET with [¹⁸ F]VC701	Subcutaneous injection of MOG ₃₅₋₅₅ /CFA and pertussis toxin in female C57BL/6J mice (8–12 weeks old)	14 days after EAE induction	clodronate • Increased [18F]VC701 SUVr in the cortex, cerebellum, striatum, hippocampus, cervical enlargement and thoracic and lumbar spinal cord	PET data confirmed by ex vivo biodistribution of [¹⁸ F]VC701 Iba1 IHC confirmed the presence of microglia/infiltrated macrophages in the same brain ROIs as PET EAE lesion visible on MRI but highly variable in volume	[189]
[¹¹ C]PBR28 [¹⁸ F]FOL (FR-β) [201] [¹⁸ F]GE-180	Investigate FR-β expression and evaluate its potential as an in vivo imaging target in comparison of TSPO	Intrastriatal injection of heat-killed BCG followed by intradermal injection of <i>Mycobacterium tuberculosis</i> -H37Ra in male Lewis rats (3–4 months old, 235±9 g)	14 and 90 days after EAE induction	• Increase in [11C]PBR28 SUVr 14 and 90 days after EAE induction • Increase in [18F]FOL SUVr, similar to [11C]PBR28 SUVr, at 14 days • [18F]FOL SUVr higher than [11C]PBR28 SUVr at 90 days	 ARG for [¹¹C]PBR28 and [¹⁸F]FOL confirmed the PET data IHC confirmed the presence of FR-β, CD68, MRC1 and iNOS staining in the same ROIs as PET, especially at 90 days 	[202] [190]



Table 7 (continued)

PET tracer *	Rational	MS model and species	Imaging time points	Main imaging findings	Additional readouts	Ref.
	Feasibility study of using TSPO-PET to detect NI in EAE and determine which cell types express TSPO	CPZ-induced EAE and/or MOG ₃₅₋₅₅ immunization in C57BL/6 mice and hGFAP/EGFP (astrocyte), CX3CR1 ⁺ /eGFP/CCR2 ⁺ /- RFP (monocyte-derived macrophages) and eGFP-expressing microglial	5 weeks after EAE induction	*Increase of [18F]-GE180 uptake in CPZ-treated mice (+36 to +65% vs control mice)	• IHC analysis revealed that TSPO mostly colocalize with microglia following CPZ • The combination CPZ and/or MOG ₃₅₋₅₅ induces the recruitment	
[¹⁸ F]GE-180	Test effect of anti-VLA-4 treatment in EAE	transgenic mice Intrastriatal injection of heat-killed BCG followed by intradermal injection of Mycobacterium tuberculosis in male Lewis rats	30, 44, 65, 86 and 142 after EAE induction	 Declining trend (p = 0.067) in [¹⁸F]GE-180-binding after 2 weeks of anti-VLA-4 mAb-treatment vs controls After 31-days of anti-VLA-4 mAb treatment, cessation of treatment increased [¹⁸F]GE-180 binding vs control group No difference between groups in TSPO 	of TSPO+ monocytes IHC confirmed the presence of Iba1 ⁺ cells in the lesion	[191]
[¹⁸ F]DPA-714	Investigate the temporal profile of NI in relation to MRI in EAE	CPZ-induced EAE in female C57Bl6 mice (8 weeks old, 19.8±1.5 g)	4 and 5–6 weeks after EAE induction	increased in EAE mice at 4 weeks and declined at 6 weeks in the CC, hippocampus and thalamus Increased T2 values in the CC of CPZ compared to control at 3 and 5 weeks Partial recovery of T2 values between weeks	Ex vivo [¹⁸ F]DPA-714 ARG confirmed the PET data IHC: during demyelination (week 3), TSPO+ cells are microglia; during remyelination, TSPO+ cells are astrocytes IHC confirmed remyelination at week 6	[193]
[¹⁸ F]GE-180	Test MS treatment laquinimod in EAE model	CPZ-induced EAE ± MOG ₃₅₋₅₅ immunization in female C57Bl6 mice (8 weeks old)	5 weeks after EAE induction	3 and 5 • Laquinimod treatment returned EAE-induced increased [18F]GE-180 uptake to control values	IHC measurements confirmed reduced NI and decrease of ND markers	[192]
[¹⁸ F]DPA-714	Feasibility study of using TSPO-PET and SPIO-MRI to detect NI in EAE and determine which cell types express TSPO	Immunization with PLP ₁₃₉₋₁₅₁ of female SJL/J mice (6 weeks old)	11 to 14 days post immunization	In	TSPO/Iba1 and F4/80/Prussian blue IHC staining suggests that microglia and macrophages are the source of [18F]DPA-714 and SPIO signal	[194]

^{*}TSPO-PET tracers and associated results are in bold.

Abbreviations: $[^{18}F]FDG$, fluorodeoxyglucose; $[^{18}F]FOL$, $[^{18}F]$ fluoride-labelled 1,4,7-triazacyclononane-1,4,7-triacetic acid conjugated folate; $[^{18}F]FSPG$, (4S)-4-(3-18F-fluoropropyl)-L-glutamate; ARG, autoradiography; BCG, Bacillus Calmette-Guérin; CC, corpus callosum; CPZ, cuprizone; EAE, experimental autoimmune encephalomyelitis; FR- β , folate receptor- β ; IHC, immunohistochemistry; iNOS, inducible nitric oxide synthase; MBP, myelin basic protein; MEDAS, N-methyl-4,4'-diaminostilbene; MRCI, mannose receptor C-type 1; ND, neurodegeneration; NI, neuroinflammation; SD, Sprague Dawley; SPIO, superparamagnetic iron oxide particles; SUV, standard uptake value; SUVr, standard uptake value ratio; VLA-4, very late antigen-4 integrin; WM, white matter; xc^- : cystine-glutamate antiporter system



neuroinflammation at the cessation of the treatment at 31 days, suggesting a dampening effect of the treatment on the pathophysiological processes. Similarly, Nedelcu et al. [192] investigated the effect of laquinimod in a mouse model of MS also using [18F]GE-180. These authors demonstrated that laquinimod was able to reverse neuroinflammation to baseline levels confirming the potential of this treatment in MS as previously described [196, 197].

Some studies used a multitracer approach to investigate different parameters simultaneously in MS models. In a model of demyelination in rats, de Paula Faria et al. [198] used [11C]-R-PK11195 for TSPO expression, [11C]MeDAS for myelin level and [18F]FDG for metabolism. While they showed no change in [18F]FDG uptake, they observed a significant increase (+37 to +84%) in [11C]-R-PK11195 uptake in the lesion where myelin binding of [11C]MeDAS was significantly decreased within a week. Similarly, Martin et al. [199] also found no change in [18F]FDG uptake in an EAE model in rats, while TSPO ([11C]-R-PK11195) was significantly increased in the cerebellum and spinal cord, and cystine-glutamate antiporter system (system xc⁻) ([¹⁸F]FSPG) was increased in the spinal cord 14 days post-EAE induction. As for the study in stroke [97], this raises the prospect of system xc being involved in neuroinflammatory processes in MS and being a potential therapeutic target. Finally, and using [18F]FOL to target folate receptor-β (FR-β) that is expressed on activated macrophages, Elo et al. investigated the use of FR-β as a potential biomarker for neuroinflammation imaging in MS in comparison with [11C]PBR28 PET. Fourteen days post-EAE induction, both [11C]PBR28 and [18F]FOL were similarly increased; however, at 90 days post-EAE induction, [18F]FOL uptake was higher than [11C]PBR28 uptake. Immunohistochemistry revealed that FR-β was expressed by both microglia and macrophages in EAE lesion; however, the different uptake of both tracers at 90 days suggests that [18F]FOL/FR-\beta imaging may be complementary of TSPO imaging in MS.

Overall, in preclinical models of MS, TSPO expression is robustly and consistently detected as it is the case in MS patients. In this context, TSPO imaging has a great potential as a readout for therapeutic response (Table 7).

General conclusion

Taken altogether, TSPO-PET imaging is highly valuable in assessing the time course, anatomical brain localization of neuroinflammation and response to treatment in a range of disease models from acute, subacute to chronic conditions. We observed that the TSPO-PET ligands that have been developed over the last 15 years to overcome the shortcomings of [11C]-R-PK11195 have been applied in a large variety of preclinical studies. To the best of our knowledge, the

differential affinity of these ligands for the human TSPO polymorphisms has still not been an issue in preclinical research nor in larger animals. Recently, newer ligands, which are not sensitive to these polymorphisms, are integrating the field. Future studies will define if these ligands present an overall gain in preclinical research over [11C]-R-PK11195 in terms of signal-to-noise ratio. Clinical studies will then have to determine if this gain is translated into clinical imaging and if they are truly insensitive to the TSPO polymorphism in human.

Overall, we can conclude that TSPO-PET imaging is a powerful tool to evaluate the neuroinflammatory response in models with strong and localized effects, such as intracerebral administered toxic lesion models (LPS, QA, 6-OHDA) and stroke models. The main advantage of these models is the reproducibility and predictiveness of the size, localization and the time window of the neuroinflammatory response as well as the known cell origin of the TSPO expression. These parameters reduce considerably the inter-animal variability and simplify the experimental design. However, the major drawback of these models of acute neuroinflammation is the limited translational generalizability for neurological disorders with a systemic or chronic pathogenesis. This limitation highlights a strength of acute LPS administration, which can be given systematically, to model sickness behaviour and peripheral increase of inflammatory cytokines on the central neuroinflammatory response. However, dramatic species differences in LPS sensitivity are a key for translational consideration. On the other hand, viral vector-induced models or transgenic animal models of neurodegenerative diseases have the merit to better reflect the clinical pathology because they are slowly progressive, even though neuronal loss is often moderated within the time window of the experimental design. However, they also generate higher intra-animal variability and are more complex to handle in their experimental design. Additionally, the neuroinflammatory response in these models is often more modest and less well characterized but actually reproduces fairly well the amplitude and characteristics of the neuroinflammatory response observed in a clinical scenario. In animal models with a low and localized neuroimmune response, the use of ex vivo or in vitro autoradiography compensates for the limited resolution and sensitivity of in vivo PET imaging. A more general limitation is the use of SUV as a pseudo-quantitative measurement to overcome the complexities of blood sampling in small animal models. However, SUV is rarely compared with gold standard measurements of V_T and/or verify the free blood fraction of the ligand. When this measure is not homogeneous between experimental groups, an important bias may be introduced when using pseudo-quantitative parameters. This supports the development and use of animal models in larger species, such as non-human primates and minipigs, to circumvent some of the difficulties encountered when using rodents (small brain and limited possibilities of arterial blood



sampling). A summary of the strengths and weaknesses of preclinical models described in this review is provided in Table 8.

Table 8 Strengths and weaknesses of preclinical models regarding TSPO-PET imaging

Model	Pros	Cons	
LPS	Intracerebral administration provides a robust neuroinflammatory response. Useful to model the impact of systemic inflammation on neurodegenerative and neuroinflammatory events	Important species differences in neuroinflammatory response after peripheral LPS challenge Differences in neuroinflammatory responses between batches of LPS	• For most models: small brain size of rodents, particularly mice, relative to the resolution of preclinical PET scanners. • Need to implement
Stroke	Robust, focal and well-defined time course of the neuroinflammatory response	Complexity and/or invasiveness of surgery (depending on model)	more clinically relevant models in larger species
	Moderate to good trans depending on the str		
AD	Amplitudes of increases in TSPO expression are similar in amplitude to what is observed in clinic	Transgenic models are only modelling the familial form of AD	
PD	Within the time window of the experimental design, neurodegeneration in viral vector-induced models is generally mild, alongside a modest and yet poorly characterized neuroinflammatory	Acute neurodegenerative models present transient neuroinflammatory response which is not representative for a chronic aspect of clinical profile	
HD	response Robust, focal, strong, rapid and well-defined time course of neuroinflammatory response (QA)	Poor to moderate translational value; invasiveness of surgery (QA)	
MS	Easy to induce, rapid neuroinflammatory response Poor to moderate transl	lational value	

Altogether, these TSPO-PET imaging studies demonstrated the implication and possible modulation of neuroinflammation by various systems in preclinical models and offered new insights into disease mechanisms and associated potential new therapeutic avenues. Additionally, they showed that these phenomena can be monitored in vivo longitudinally using preclinical PET alone (using one or several radiotracers) or in combination with other non-invasive imaging techniques. Importantly, these studies confirmed further the true potential of preclinical PET imaging and the still undeniable value of TSPO-PET to image neuroinflammation even though TSPO might not be seen as the ideal direct biomarker for neuroinflammation.

Interestingly, all these preclinical studies highlight the strengths and values of preclinical models in which it is possible to investigate the detailed cellular expression of TSPO (in microglia, macrophages, astrocytes and endothelial cells) as well as the meaning of such overexpression in the context of the cellular phenotype (pro- vs anti-inflammatory) and in relation with the immune response observed in these disease models, something that can be done only at the latest stage of disease in human samples.

There are many arguments that can be raised regarding the imperfection of TSPO as a biomarker of neuroinflammation since TSPO is not directly involved in the inflammatory responses as are a wide range of molecule such as cytokines, chemokines, P2X7 receptors, inflammasomes, etc. Nevertheless, until other biomarkers and associated radiotracers can fulfil the gap of TSPO shortfall, TSPO remains a tool of choice to investigate and understand neuroinflammation and response to anti-inflammatory treatment in animal models, and it still has an incredible value as a translational target for neuroinflammation imaging in clinic.

Declarations

Conflicts of interest HB has received funding from GSK. GSK was not involved in any way in the redaction of this review.

Open Access This article is licensed under a Creative Commons Attribution 4.0 International License, which permits use, sharing, adaptation, distribution and reproduction in any medium or format, as long as you give appropriate credit to the original author(s) and the source, provide a link to the Creative Commons licence, and indicate if changes were made. The images or other third party material in this article are included in the article's Creative Commons licence, unless indicated otherwise in a credit line to the material. If material is not included in the article's Creative Commons licence and your intended use is not permitted by statutory regulation or exceeds the permitted use, you will need to obtain permission directly from the copyright holder. To view a copy of this licence, visit http://creativecommons.org/licenses/by/4.0/.



References

- Benavides J, Malgouris C, Imbault F, Begassat F, Uzan A, Renault C, et al. "Peripheral type" benzodiazepine binding sites in rat adrenals: binding studies with [3H]PK 11195 and autoradiographic localization. Arch Int Pharmacodyn Ther. 1983;266: 38–49.
- Le Fur G, Vaucher N, Perrier ML, Flamier A, Benavides J, Renault C, et al. Differentiation between two ligands for peripheral benzodiazepine binding sites, [3H]RO5-4864 and [3H]PK 11195, by thermodynamic studies. Life Sci. 1983;33:449–57.
- Benavides J, Guilloux F, Rufat P, Uzan A, Renault C, Dubroeucq MC, et al. In vivo labelling in several rat tissues of 'peripheral type' benzodiazepine binding sites. Eur J Pharmacol. 1984;99:1–7.
- Benavides J, Fage D, Carter C, Scatton B. Peripheral type benzodiazepine binding sites are a sensitive indirect index of neuronal damage. Brain Res. 1987;421(1-2):167–72. https://doi.org/10. 1016/0006-8993(87)91287-x.
- Dubois A, Benavides J, Peny B, Duverger D, Fage D, Gotti B, et al. Imaging of primary and remote ischaemic and excitotoxic brain lesions. An autoradiographic study of peripheral type benzodiazepine binding sites in the rat and cat. Brain Res. 1988;445(1):77–90. https://doi.org/10.1016/0006-8993(88) 91076-1.
- Black KL, Ikezaki K, Toga AW. Imaging of brain tumors using peripheral benzodiazepine receptor ligands. J Neurosurg. 1989;71: 113–8.
- Benavides J, Dubois A, Gotti B, Bourdiol F, Scatton B. Cellular distribution of omega 3 (peripheral type benzodiazepine) binding sites in the normal and ischaemic rat brain: an autoradiographic study with the photoaffinity ligand [3H]PK 14105. Neurosci Lett. 1990;114(1):32–8. https://doi.org/10.1016/0304-3940(90)90424-8.
- Benavides J, Capdeville C, Dauphin F, Dubois A, Duverger D, Fage D, et al. The quantification of brain lesions with an ω₃ site ligand: a critical analysis of animal models of cerebral ischaemia and neurodegeneration. Brain Res. 1990;522:275–89.
- Pappata S, Cornu P, Samson Y, Prenant C, Benavides J, Scatton B, et al. PET study of carbon-11-PK 11195 binding to peripheral type benzodiazepine sites in glioblastoma: a case report. J Nucl Med. 1991;32(8):1608–10.
- Bergstrom M, Mosskin M, Ericson K, Ehrin E, Thorell JO, von Holst H, et al. Peripheral benzodiazepine binding sites in human gliomas evaluated with positron emission tomography. Acta Radiol Suppl. 1986;369:409–11.
- Stephenson DT, Schober DA, Smalstig EB, Mincy RE, Gehlert DR, Clemens JA. Peripheral benzodiazepine receptors are colocalized with activated microglia following transient global forebrain ischemia in the rat. J Neurosci. 1995;15(7 Pt 2):5263– 74.
- Banati RB, Myers R, Kreutzberg GW. PK ('peripheral benzodiazepine')-binding sites in the CNS indicate early and discrete brain lesions: microautoradiographic detection of [3H]PK11195 binding to activated microglia. J Neurocytol. 1997;26:77–82.
- Vowinckel E, Reutens D, Becher B, Verge G, Evans A, Owens T, et al. PK11195 binding to the peripheral benzodiazepine receptor as a marker of microglia activation in multiple sclerosis and experimental autoimmune encephalomyelitis. J Neurosci Res. 1997;50:345–53.
- Banati RB, Goerres GW, Myers R, Gunn RN, Turkheimer FE, Kreutzberg GW, et al. [11C](R)-PK11195 positron emission tomography imaging of activated microglia in vivo in Rasmussen's encephalitis. Neurology. 1999;53(9):2199–203. https://doi.org/ 10.1212/wnl.53.9.2199.

- Brown GC. The endotoxin hypothesis of neurodegeneration. J Neuroinflammation. 2019;16(1):180. https://doi.org/10.1186/ s12974-019-1564-7.
- Qin L, Wu X, Block ML, Liu Y, Breese GR, Hong JS, et al. Systemic LPS causes chronic neuroinflammation and progressive neurodegeneration. Glia. 2007;55(5):453–62. https://doi.org/10. 1002/glia.20467.
- Vargas-Caraveo A, Sayd A, Maus SR, Caso JR, Madrigal JLM, Garcia-Bueno B, et al. Lipopolysaccharide enters the rat brain by a lipoprotein-mediated transport mechanism in physiological conditions. Sci Rep. 2017;7(1):13113. https://doi.org/10.1038/s41598-017-13302-6.
- Furube E, Kawai S, Inagaki H, Takagi S, Miyata S. Brain regiondependent heterogeneity and dose-dependent difference in transient microglia population increase during lipopolysaccharideinduced inflammation. Sci Rep. 2018;8(1):2203. https://doi.org/ 10.1038/s41598-018-20643-3.
- Hoogland IC, Houbolt C, van Westerloo DJ, van Gool WA, van de Beek D. Systemic inflammation and microglial activation: systematic review of animal experiments. J Neuroinflammation. 2015;12(1):114. https://doi.org/10.1186/s12974-015-0332-6.
- Lopes PC. LPS and neuroinflammation: a matter of timing. Inflammopharmacology. 2016;24(5):291–3. https://doi.org/10. 1007/s10787-016-0283-2.
- Ota M, Ogura J, Ogawa S, Kato K, Matsuda H, Kunugi H. A single intraperitoneal injection of endotoxin changes glial cells in rats as revealed by positron emission tomography using [(11)C]PK11195. Nucl Med Mol Imaging. 2018;52(3):224–8. https://doi.org/10.1007/s13139-017-0510-9.
- Schildt A, Walker MD, Dinelle K, Miao Q, Schulzer M, O'Kusky J, et al. Single inflammatory trigger leads to neuroinflammation in LRRK2 rodent model without degeneration of dopaminergic neurons. J Parkinsons Dis. 2019;9(1):121–39. https://doi.org/10.3233/JPD-181446.
- Schedlowski M, Engler H, Grigoleit J-S. Endotoxin-induced experimental systemic inflammation in humans: a model to disentangle immune-to-brain communication. Brain Behav Immun. 2014;35:1–8. https://doi.org/10.1016/j.bbi.2013.09.015.
- Hannestad J, Gallezot JD, Schafbauer T, Lim K, Kloczynski T, Morris ED, et al. Endotoxin-induced systemic inflammation activates microglia: [(1)(1)C]PBR28 positron emission tomography in nonhuman primates. Neuroimage. 2012;63(1):232–9. https://doi.org/10.1016/j.neuroimage.2012.06.055.
- Sandiego CM, Gallezot JD, Pittman B, Nabulsi N, Lim K, Lin SF, et al. Imaging robust microglial activation after lipopolysaccharide administration in humans with PET. Proc Natl Acad Sci U S A. 2015;112(40):12468–73. https://doi.org/10.1073/pnas.1511003112.
- Hillmer AT, Holden D, Fowles K, Nabulsi N, West BL, Carson RE, et al. Microglial depletion and activation: a [11C]PBR28 PET study in nonhuman primates. EJNMMI Res. 2017;7(1):59. https:// doi.org/10.1186/s13550-017-0305-0.
- Murtaj V, Belloli S, Di Grigoli G, Pannese M, Ballarini E, Rodriguez-Menendez V, et al. Age and sex influence the neuroinflammatory response to a peripheral acute LPS challenge. Front Aging Neurosci. 2019;11:299. https://doi.org/10.3389/fnagi. 2019.00299.
- Kim WG, Mohney RP, Wilson B, Jeohn GH, Liu B, Hong JS. Regional difference in susceptibility to lipopolysaccharideinduced neurotoxicity in the rat brain: role of microglia. J Neurosci. 2000;20(16):6309–16.
- Ito F, Toyama H, Kudo G, Suzuki H, Hatano K, Ichise M, et al. Two activated stages of microglia and PET imaging of peripheral benzodiazepine receptors with [(11)C]PK11195 in rats. Ann Nucl Med. 2010;24(3):163–9. https://doi.org/10.1007/s12149-009-0339-0.



- Tournier BB, Tsartsalis S, Ceyzeriat K, Medina Z, Fraser BH, Gregoire MC, et al. Fluorescence-activated cell sorting to reveal the cell origin of radioligand binding. J Cereb Blood Flow Metab. 2020;40(6):1242-55. https://doi.org/10.1177/0271678X19860408.
- Vignal N, Boulay AC, San C, Cohen-Salmon M, Rizzo-Padoin N, Sarda-Mantel L, et al. Astroglial connexin 43 deficiency protects against LPS-induced neuroinflammation: a TSPO brain microPET study with [(18)F]FEPPA. Cells. 2020;9(2). https://doi.org/10. 3390/cells9020389.
- Liddelow SA, Guttenplan KA, Clarke LE, Bennett FC, Bohlen CJ, Schirmer L, et al. Neurotoxic reactive astrocytes are induced by activated microglia. Nature. 2017;541(7638):481–7. https://doi. org/10.1038/nature21029.
- Pannell M, Economopoulos V, Wilson TC, Kersemans V, Isenegger PG, Larkin JR, et al. Imaging of translocator protein upregulation is selective for pro-inflammatory polarized astrocytes and microglia. Glia. 2020;68(2):280–97. https://doi.org/10. 1002/glia.23716.
- Ory D, Planas A, Dresselaers T, Gsell W, Postnov A, Celen S, et al. PET imaging of TSPO in a rat model of local neuroinflammation induced by intracerebral injection of lipopolysaccharide. Nucl Med Biol. 2015;42(10):753–61. https://doi.org/10.1016/j.nucmedbio.2015.06.010.
- Pottier G, Gomez-Vallejo V, Padro D, Boisgard R, Dolle F, Llop J, et al. PET imaging of cannabinoid type 2 receptors with [(11)C]A-836339 did not evidence changes following neuroinflammation in rats. J Cereb Blood Flow Metab. 2017;37(3): 1163–78. https://doi.org/10.1177/0271678X16685105.
- Owen DR, Narayan N, Wells L, Healy L, Smyth E, Rabiner EA, et al. Pro-inflammatory activation of primary microglia and macrophages increases 18 kDa translocator protein expression in rodents but not humans. J Cereb Blood Flow Metab. 2017;37(8): 2679–90. https://doi.org/10.1177/0271678x17710182.
- Kim K, Kim H, Bae SH, Lee SY, Kim YH, Na J, et al. [(18)F]CB251 PET/MR imaging probe targeting translocator protein (TSPO) independent of its polymorphism in a neuroinflammation model. Theranostics. 2020;10(20):9315–31. https://doi.org/10.7150/thno.46875.
- 38. Moon BS, Kim BS, Park C, Jung JH, Lee YW, Lee H-Y, et al. [18F] Fluoromethyl-PBR28 as a potential radiotracer for TSPO: preclinical comparison with [11C] PBR28 in a rat model of neuroinflammation. Bioconjug Chem. 2014;25(2):442–50.
- Venneti S, Lopresti BJ, Wang G, Slagel SL, Mason NS, Mathis CA, et al. A comparison of the high-affinity peripheral benzodiazepine receptor ligands DAA1106 and (R)-PK11195 in rat models of neuroinflammation: implications for PET imaging of microglial activation. J Neurochem. 2007;102(6):2118–31. https://doi.org/10.1111/j.1471-4159.2007.04690.x.
- Sridharan S, Lepelletier FX, Trigg W, Banister S, Reekie T, Kassiou M, et al. Comparative evaluation of Three TSPO PET radiotracers in a LPS-induced model of mild neuroinflammation in rats. Molec imag Biol. 2017;19(1):77–89. https://doi.org/10. 1007/s11307-016-0984-3.
- 41. Berdyyeva T, Xia C, Taylor N, He Y, Chen G, Huang C, et al. PET imaging of the P2X7 ion channel with a novel tracer [(18)F]JNJ-64413739 in a rat model of neuroinflammation. Molec imag Biol. 2019;21(5):871–8. https://doi.org/10.1007/s11307-018-01313-2.
- Flores-Martinez YM, Fernandez-Parrilla MA, Ayala-Davila J, Reyes-Corona D, Blanco-Alvarez VM, Soto-Rojas LO, et al. Acute neuroinflammatory response in the substantia nigra pars compacta of rats after a local injection of lipopolysaccharide. J Immunol Res. 2018;2018:1838921. https://doi.org/10.1155/ 2018/1838921.

- Choi DY, Liu M, Hunter RL, Cass WA, Pandya JD, Sullivan PG, et al. Striatal neuroinflammation promotes Parkinsonism in rats. PLoS One. 2009;4(5):e5482. https://doi.org/10.1371/journal. pone.0005482.
- 44. Ory D, Postnov A, Koole M, Celen S, de Laat B, Verbruggen A, et al. Quantification of TSPO overexpression in a rat model of local neuroinflammation induced by intracerebral injection of LPS by the use of [(18)F]DPA-714 PET. Eur J Nucl Med Mol Imaging. 2016;43(1):163–72. https://doi.org/10.1007/s00259-015-3172-9.
- Vignal N, Cisternino S, Rizzo-Padoin N, San C, Hontonnou F, Gele T, et al. [(18)F]FEPPA a TSPO radioligand: optimized radiosynthesis and evaluation as a PET radiotracer for brain inflammation in a peripheral LPS-Injected mouse model. Molecules (Basel, Switzerland). 2018;23(6). https://doi.org/10.3390/ molecules23061375.
- Woodcock EA, Schain M, Cosgrove KP, Hillmer AT. Quantification of [(11)C]PBR28 data after systemic lipopolysaccharide challenge. EJNMMI Res. 2020;10(1):19. https://doi.org/ 10.1186/s13550-020-0605-7.
- Zhang Z, Jyoti A, Balakrishnan B, Williams M, Singh S, Chugani DC, et al. Trajectory of inflammatory and microglial activation markers in the postnatal rabbit brain following intrauterine endotoxin exposure. Neurobiol Dis. 2018;111:153–62. https://doi.org/10.1016/j.nbd.2017.12.013.
- Hieu Tran V, Park H, Park J, Kwon YD, Kang S, Ho Jung J, et al. Synthesis and evaluation of novel potent TSPO PET ligands with 2-phenylpyrazolo[1,5-a]pyrimidin-3-yl acetamide. Bioorg Med Chem. 2019;27(18):4069–80. https://doi.org/10.1016/j.bmc. 2019.07.036.
- Kwon YD, Kang S, Park H, Cheong IK, Chang KA, Lee SY, et al. Novel potential pyrazolopyrimidine based translocator protein ligands for the evaluation of neuroinflammation with PET. Eur J Med Chem. 2018;159:292–306. https://doi.org/10.1016/j.ejmech. 2018.09.069.
- Moon BS, Jung JH, Park HS, Contino M, Denora N, Lee BC, et al. Preclinical comparison study between [(18)F]fluoromethyl-PBR28 and its deuterated analog in a rat model of neuroinflammation. Bioorg Med Chem Lett. 2018;28(17):2925–9. https://doi. org/10.1016/j.bmcl.2018.07.011.
- Vieira IF, Ory D, Casteels C, Lima FRA, Van Laere K, Bormans G, et al. Volume-of-interest-based supervised cluster analysis for pseudo-reference region selection in [(18)F]DPA-714 PET imaging of the rat brain. EJNMMI Res. 2018;8(1):112. https://doi.org/10.1186/s13550-018-0467-4.
- Dickens AM, Vainio S, Marjamaki P, Johansson J, Lehtiniemi P, Rokka J, et al. Detection of microglial activation in an acute model of neuroinflammation using PET and radiotracers 11C-(R)-PK11195 and 18F-GE-180. J Nucl Med. 2014;55(3):466-72. https://doi.org/10.2967/jnumed.113.125625.
- Buttini M, Sauter A, Boddeke HW. Induction of interleukin-1 beta mRNA after focal cerebral ischaemia in the rat. Brain Res Mol Brain Res. 1994;23(1-2):126–34. https://doi.org/10.1016/0169-328x(94)90218-6.
- Grau AJ. Infection, inflammation, and cerebrovascular ischemia.
 Neurology. 1997;49(5 Suppl 4):S47–51. https://doi.org/10.1212/wnl.49.5 suppl 4.s47.
- Touzani O, Boutin H, Chuquet J, Rothwell N. Potential mechanisms of interleukin-1 involvement in cerebral ischaemia. J Neuroimmunol. 1999;100(1-2):203–15. https://doi.org/10.1016/s0165-5728(99)00202-7.
- Benavides J, Cornu P, Dennis T, Dubois A, Hauw JJ, MacKenzie ET, et al. Imaging of human brain lesions with an omega 3 site radioligand. Ann Neurol. 1988;24(6):708–12. https://doi.org/10.1002/ana.410240603.



- Pappata S, Levasseur M, Gunn RN, Myers R, Crouzel C, Syrota A, et al. Thalamic microglial activation in ischemic stroke detected in vivo by PET and [11C]PK11195. Neurology. 2000;55:1052–4.
- Gerhard A, Schwarz J, Myers R, Wise R, Banati RB. Evolution of microglial activation in patients after ischemic stroke: a [11C](R)-PK11195 PET study. Neuroimage. 2005;24(2):591–5. https://doi. org/10.1016/j.neuroimage.2004.09.034.
- Price CJ, Wang D, Menon DK, Guadagno JV, Cleij M, Fryer T, et al. Intrinsic activated microglia map to the peri-infarct zone in the subacute phase of ischemic stroke. Stroke. 2006;37(7):1749– 53. https://doi.org/10.1161/01.STR.0000226980.95389.0b.
- Boutin H, Pinborg LH. TSPO imaging in stroke: from animal models to human subjects. Clin Transl Imaging. 2015;3(6):423– 35. https://doi.org/10.1007/s40336-015-0146-7.
- Petit-Taboue MC, Baron JC, Barre L, Travere JM, Speckel D, Camsonne R, et al. Brain kinetics and specific binding of [11C]PK 11195 to omega 3 sites in baboons: positron emission tomography study. Eur J Pharmacol. 1991;200(2-3):347–51. https://doi.org/10.1016/0014-2999(91)90594-g.
- 62. Sette G, Baron JC, Young AR, Miyazawa H, Tillet I, Barre L, et al. *In vivo* mapping of brain benzodiazepine receptor changes by positron emission tomography after focal ischemia in the anesthetized baboon. Stroke. 1993;24(12):2046–57; discussion 57-8. https://doi.org/10.1161/01.str.24.12.2046.
- Imaizumi M, Kim HJ, Zoghbi SS, Briard E, Hong J, Musachio JL, et al. PET imaging with [(11)C]PBR28 can localize and quantify upregulated peripheral benzodiazepine receptors associated with cerebral ischemia in rat. Neurosci Lett. 2007;411:200–5.
- 64. Boutin H, Prenant C, Maroy R, Galea J, Greenhalgh AD, Smigova A, et al. [¹⁸F]DPA-714: direct comparison with [¹¹C]PK11195 in a model of cerebral ischemia in rats. PLoS One. 2013;8(2): e56441. https://doi.org/10.1371/journal.pone.0056441.
- Martin A, Boisgard R, Theze B, Van Camp N, Kuhnast B, Damont A, et al. Evaluation of the PBR/TSPO radioligand [(18)F]DPA-714 in a rat model of focal cerebral ischemia. J Cereb Blood Flow Metab. 2010;30(1):230–41. https://doi.org/ 10.1038/jcbfm.2009.205.
- Tiwari AK, Ji B, Yui J, Fujinaga M, Yamasaki T, Xie L, et al. [18F]FEBMP: positron emission tomography imaging of TSPO in a model of neuroinflammation in rats, and in vitro autoradiograms of the human brain. Theranostics. 2015;5(9):961–9. https://doi.org/10.7150/thno.12027.
- Boutin H, Murray K, Pradillo J, Maroy R, Smigova A, Gerhard A, et al. 18F-GE-180: a novel TSPO radiotracer compared to 11C-R-PK11195 in a preclinical model of stroke. Eur J Nucl Med Mol Imaging. 2015;42(3):503–11. https://doi.org/10.1007/s00259-014-2939-8.
- Buchert R, Dirks M, Schutze C, Wilke F, Mamach M, Wirries AK, et al. Reliable quantification of (18)F-GE-180 PET neuroin-flammation studies using an individually scaled population-based input function or late tissue-to-blood ratio. Eur J Nucl Med Mol Imaging. 2020;47(12):2887–900. https://doi.org/10.1007/s00259-020-04810-1.
- de Groot M, Patel N, Manavaki R, Janiczek RL, Bergstrom M, Ostor A, et al. Quantifying disease activity in rheumatoid arthritis with the TSPO PET ligand (18)F-GE-180 and comparison with (18)F-FDG and DCE-MRI. EJNMMI Res. 2019;9(1):113. https:// doi.org/10.1186/s13550-019-0576-8.
- Sridharan S, Raffel J, Nandoskar A, Record C, Brooks DJ, Owen D, et al. Confirmation of specific binding of the 18-kDa translocator protein (TSPO) radioligand [(18)F]GE-180: a blocking study using XBD173 in multiple sclerosis normal appearing white and grey matter. Molec imag Biol. 2019;21(5): 935–44. https://doi.org/10.1007/s11307-019-01323-8.
- Unterrainer M, Fleischmann DF, Vettermann F, Ruf V, Kaiser L, Nelwan D, et al. TSPO PET, tumour grading and molecular

- genetics in histologically verified glioma: a correlative (18)F-GE-180 PET study. Eur J Nucl Med Mol Imaging. 2020;47(6): 1368–80. https://doi.org/10.1007/s00259-019-04491-5.
- 72. Vettermann FJ, Unterrainer M, Ruf V, Fleischmann DF, Rupprecht R, Forbrig R, et al. Dual PET imaging of an H3K27M-mutant glioma with 18F-GE-180 and 18F-FET PET. Clin Nucl Med. 2020;45(12):992–3. https://doi.org/10.1097/RLU.0000000000003331.
- Volk S, Unterrainer M, Albert NL, Havla J, Gerdes LA, Schumacher M, et al. TSPO PET with 18F-GE-180 to differentiate variants of multiple sclerosis: relapsing-remitting multiple sclerosis, tumefactive demyelination, and Balo's concentric sclerosis. Clin Nucl Med. 2020;45(10):e447–e8. https://doi.org/10. 1097/RLU.0000000000003220.
- Fujinaga M, Luo R, Kumata K, Zhang Y, Hatori A, Yamasaki T, et al. Development of a (18)F-labeled radiotracer with improved brain kinetics for positron emission tomography imaging of translocator protein (18 kDa) in ischemic brain and glioma. J Med Chem. 2017;60(9):4047–61. https://doi.org/10.1021/acs.jmedchem.7b00374.
- Fujinaga M, Kumata K, Zhang Y, Hatori A, Yamasaki T, Mori W, et al. Synthesis of two novel [(18)F]fluorobenzene-containing radiotracers via spirocyclic iodonium ylides and positron emission tomography imaging of translocator protein (18 kDa) in ischemic brain. Org Biomol Chem. 2018;16(37):8325–35. https://doi.org/10.1039/c8ob01700j.
- Pulagam KR, Colas L, Padro D, Plaza-Garcia S, Gomez-Vallejo V, Higuchi M, et al. Evaluation of the novel TSPO radiotracer [(18)F] VUIIS1008 in a preclinical model of cerebral ischemia in rats. EJNMMI Res. 2017;7(1):93. https://doi.org/10.1186/s13550-017-0343-7.
- Tang D, Fujinaga M, Hatori A, Zhang Y, Yamasaki T, Xie L, et al. Evaluation of the novel TSPO radiotracer 2-(7-butyl-2-(4-(2-[(18)F]fluoroethoxy)phenyl)-5-methylpyrazolo[1,5-a]pyrimidin-3-yl)-N,N-diethylacetamide in a preclinical model of neuroinflammation. Eur J Med Chem. 2018;150:1–8. https://doi.org/10.1016/j.ejmech.2018.02.076.
- Wang L, Cheng R, Fujinaga M, Yang J, Zhang Y, Hatori A, et al. A facile radiolabeling of [(18)F]FDPA via spirocyclic iodonium ylides: preliminary PET imaging studies in preclinical models of neuroinflammation. J Med Chem. 2017;60(12):5222–7. https:// doi.org/10.1021/acs.jmedchem.7b00432.
- Keller T, Krzyczmonik A, Forsback S, Picon FRL, Kirjavainen AK, Takkinen J, et al. Radiosynthesis and preclinical evaluation of [(18)F]F-DPA, a novel pyrazolo[1,5a]pyrimidine acetamide TSPO radioligand, in healthy Sprague Dawley rats. Molec imag Biol. 2017;19(5):736–45. https://doi.org/10.1007/s11307-016-1040-z.
- Chaney A, Cropper HC, Johnson EM, Lechtenberg KJ, Peterson TC, Stevens MY, et al. (11)C-DPA-713 versus (18)F-GE-180: a preclinical comparison of translocator protein 18 kDa PET tracers to visualize acute and chronic neuroinflammation in a mouse model of ischemic stroke. J Nucl Med. 2019;60(1):122–8. https://doi.org/10.2967/jnumed.118.209155.
- de Lange C, Solberg R, Holtedahl JE, Tulipan A, Barlinn J, Trigg W, et al. Dynamic TSPO-PET for assessing early effects of cerebral hypoxia and resuscitation in new born pigs. Nucl Med Biol. 2018;66:49–57. https://doi.org/10.1016/j.nucmedbio.2018.08. 004.
- Thomas C, Vercouillie J, Domene A, Tauber C, Kassiou M, Guilloteau D, et al. Detection of neuroinflammation in a rat model of subarachnoid hemorrhage using [18F]DPA-714 PET imaging. Mol Imaging. 2016;15. https://doi.org/10.1177/ 1536012116639189.
- Toth M, Little P, Arnberg F, Haggkvist J, Mulder J, Halldin C, et al. Acute neuroinflammation in a clinically relevant focal cortical



- ischemic stroke model in rat: longitudinal positron emission tomography and immunofluorescent tracking. Brain Struct Funct. 2016;221(3):1279–90. https://doi.org/10.1007/s00429-014-0970-y.
- Miyajima N, Ito M, Rokugawa T, Iimori H, Momosaki S, Omachi S, et al. Detection of neuroinflammation before selective neuronal loss appearance after mild focal ischemia using [(18)F]DPA-714 imaging. EJNMMI Res. 2018;8(1):43. https://doi.org/10.1186/s13550-018-0400-x.
- Walter HL, Walberer M, Rueger MA, Backes H, Wiedermann D, Hoehn M, et al. In vivo analysis of neuroinflammation in the late chronic phase after experimental stroke. Neuroscience. 2015;292: 71–80. https://doi.org/10.1016/j.neuroscience.2015.02.024.
- Al-Khishman NU, Qi Q, Roseborough AD, Levit A, Allman BL, Anazodo UC, et al. TSPO PET detects acute neuroinflammation but not diffuse chronically activated MHCII microglia in the rat. EJNMMI Res. 2020;10(1):113. https://doi.org/10.1186/s13550-020-00699-x.
- Backes H, Walberer M, Ladwig A, Rueger MA, Neumaier B, Endepols H, et al. Glucose consumption of inflammatory cells masks metabolic deficits in the brain. Neuroimage. 2016;128: 54–62. https://doi.org/10.1016/j.neuroimage.2015.12.044.
- Ichiya Y, Kuwabara Y, Sasaki M, Yoshida T, Akashi Y, Murayama S, et al. FDG-PET in infectious lesions: the detection and assessment of lesion activity. Ann Nucl Med. 1996;10(2): 185–91. https://doi.org/10.1007/BF03165391.
- Oyen WJ, Mansi L. FDG-PET in infectious and inflammatory disease. Eur J Nucl Med Mol Imaging. 2003;30(11):1568–70. https://doi.org/10.1007/s00259-003-1359-y.
- Lawal I, Sathekge M. F-18 FDG PET/CT imaging of cardiac and vascular inflammation and infection. Br Med Bull. 2016;120(1): 55–74. https://doi.org/10.1093/bmb/ldw035.
- Henderson F, Hart PJ, Pradillo JM, Kassiou M, Christie L, Williams KJ, et al. Multi-modal imaging of long-term recovery post-stroke by positron emission tomography and matrix-assisted laser desorption/ionisation mass spectrometry. Rapid Commun Mass Spectrom. 2018;32(9):721–9. https://doi.org/10.1002/rcm. 8090.
- Lepelletier FX, Vandesquille M, Asselin MC, Prenant C, Robinson AC, Mann DMA, et al. Evaluation of (18)F-IAM6067 as a sigma-1 receptor PET tracer for neurodegeneration in vivo in rodents and in human tissue. Theranostics. 2020;10(18):7938–55. https://doi.org/10.7150/thno.47585.
- 93. Hosoya T, Fukumoto D, Kakiuchi T, Nishiyama S, Yamamoto S, Ohba H, et al. In vivo TSPO and cannabinoid receptor type 2 availability early in post-stroke neuroinflammation in rats: a positron emission tomography study. J Neuroinflammation. 2017;14(1):69. https://doi.org/10.1186/s12974-017-0851-4.
- 94. Zinnhardt B, Viel T, Wachsmuth L, Vrachimis A, Wagner S, Breyholz HJ, et al. Multimodal imaging reveals temporal and spatial microglia and matrix metalloproteinase activity after experimental stroke. J Cereb Blood Flow Metab. 2015;35(11):1711–21. https://doi.org/10.1038/jcbfm.2015.149.
- Barca C, Foray C, Hermann S, Doring C, Schafers M, Jacobs AH, et al. Characterization of the inflammatory post-ischemic tissue by full volumetric analysis of a multimodal imaging dataset. Neuroimage. 2020;222:117217. https://doi.org/10.1016/j. neuroimage.2020.117217.
- Martin A, Szczupak B, Gomez-Vallejo V, Domercq M, Cano A, Padro D, et al. In vivo PET imaging of the alpha4beta2 nicotinic acetylcholine receptor as a marker for brain inflammation after cerebral ischemia. J Neurosci. 2015;35(15):5998–6009. https:// doi.org/10.1523/JNEUROSCI.3670-14.2015.
- Domercq M, Szczupak B, Gejo J, Gomez-Vallejo V, Padro D, Gona KB, et al. PET imaging with [(18)F]FSPG evidences the role of system xc(-) on brain inflammation following cerebral

- ischemia in rats. Theranostics. 2016;6(11):1753–67. https://doi.org/10.7150/thno.15616.
- Moraga A, Gomez-Vallejo V, Cuartero MI, Szczupak B, San Sebastian E, Markuerkiaga I, et al. Imaging the role of toll-like receptor 4 on cell proliferation and inflammation after cerebral ischemia by positron emission tomography. J Cereb Blood Flow Metab. 2016;36(4):702-8. https://doi.org/10.1177/ 0271678X15627657.
- Joya A, Ardaya M, Montilla A, Garbizu M, Plaza-Garcia S, Gomez-Vallejo V, et al. In vivo multimodal imaging of adenosine A1 receptors in neuroinflammation after experimental stroke. Theranostics. 2021;11(1):410–25. https://doi.org/10.7150/thno. 51046.
- Braun R, Klein R, Walter HL, Ohren M, Freudenmacher L, Getachew K, et al. Transcranial direct current stimulation accelerates recovery of function, induces neurogenesis and recruits oligodendrocyte precursors in a rat model of stroke. Exp Neurol. 2016;279:127–36. https://doi.org/10.1016/j.expneurol.2016.02.018.
- 101. Tan C, Zhao S, Higashikawa K, Wang Z, Kawabori M, Abumiya T, et al. [(18)F]DPA-714 PET imaging shows immunomodulatory effect of intravenous administration of bone marrow stromal cells after transient focal ischemia. EJNMMI Res. 2018;8(1):35. https://doi.org/10.1186/s13550-018-0392-6.
- 102. Schmaljohann J, Minnerop M, Karwath P, Gundisch D, Falkai P, Guhlke S, et al. Imaging of central nAChReceptors with 2-[18F]F-A85380: optimized synthesis and in vitro evaluation in Alzheimer's disease. Appl Radiat Isot. 2004;61(6):1235–40. https://doi.org/10.1016/j.apradiso.2004.02.026.
- 103. Mittra ES, Koglin N, Mosci C, Kumar M, Hoehne A, Keu KV, et al. Pilot preclinical and clinical evaluation of (4S)-4-(3-[18F]fluoropropyl)-L-glutamate (18F-FSPG) for PET/CT imaging of intracranial malignancies. PLoS One. 2016;11(2):e0148628. https://doi.org/10.1371/journal.pone.0148628.
- 104. Evens N, Vandeputte C, Coolen C, Janssen P, Sciot R, Baekelandt V, et al. Preclinical evaluation of [11C]NE40, a type 2 cannabinoid receptor PET tracer. Nucl Med Biol. 2012;39(3):389–99. https://doi.org/10.1016/j.nucmedbio.2011.09.005.
- 105. Kumata K, Zhang Y, Fujinaga M, Ohkubo T, Mori W, Yamasaki T, et al. [(18)F]DAA1106: automated radiosynthesis using spirocyclic iodonium ylide and preclinical evaluation for positron emission tomography imaging of translocator protein (18kDa). Bioorg Med Chem. 2018;26(17):4817–22. https://doi.org/10.1016/j.bmc.2018.08.017.
- 106. Wagner S, Faust A, Breyholz HJ, Schober O, Schafers M, Kopka K. The MMP inhibitor (R)-2-(N-benzyl-4-(2-[18F]fluoroethoxy)phenylsulphonamido)-N-hydroxy-3-methylbuta namide: Improved precursor synthesis and fully automated radiosynthesis. Appl Radiat Isot. 2011;69(6):862–8. https://doi.org/10.1016/j.apradiso.2011.02.038.
- 107. Bauer A, Holschbach MH, Cremer M, Weber S, Boy C, Shah NJ, et al. Evaluation of 18F-CPFPX, a novel adenosine A1 receptor ligand: in vitro autoradiography and high-resolution small animal PET. J Nucl Med. 2003;44(10):1682–9.
- Brugg B, Dubreuil YL, Huber G, Wollman EE, Delhaye-Bouchaud N, Mariani J. Inflammatory processes induce beta-amyloid precursor protein changes in mouse brain. Proc Natl Acad Sci U S A. 1995;92(7):3032–5. https://doi.org/10.1073/pnas.92.7.3032.
- Johnston H, Boutin H, Allan SM. Assessing the contribution of inflammation in models of Alzheimer's disease. Biochem Soc Trans. 2011;39(4):886–90. https://doi.org/10.1042/BST0390886.
- Verkhratsky A, Parpura V, Rodriguez-Arellano JJ, Zorec R. Astroglia in Alzheimer's Disease. Adv Exp Med Biol. 2019;1175:273–324. https://doi.org/10.1007/978-981-13-9913-8 11.



- Rodriguez JJ, Butt AM, Gardenal E, Parpura V, Verkhratsky A. Complex and differential glial responses in Alzheimer's disease and ageing. Curr Alzheimer Res. 2016;13(4):343–58. https://doi. org/10.2174/1567205013666160229112911.
- Dahm R. Alzheimer's discovery. Curr Biol. 2006;16(21):R906– 10. https://doi.org/10.1016/j.cub.2006.09.056.
- Chaney A, Williams SR, Boutin H. In vivo molecular imaging of neuroinflammation in Alzheimer's disease. J Neurochem. 2019;149(4):438–51. https://doi.org/10.1111/jnc.14615.
- Lopez-Picon FR, Snellman A, Eskola O, Helin S, Solin O, Haaparanta-Solin M, et al. Neuroinflammation appears early on PET imaging and then plateaus in a mouse model of Alzheimer disease. J Nucl Med. 2018;59(3):509–15. https://doi.org/10.2967/ inumed.117.197608.
- 115. Keller T, Lopez-Picon FR, Krzyczmonik A, Forsback S, Takkinen JS, Rajander J, et al. Comparison of high and low molar activity TSPO tracer [(18)F]F-DPA in a mouse model of Alzheimer's disease. J Cereb Blood Flow Metab. 2020;40(5):1012–20. https://doi.org/10.1177/0271678X19853117.
- Sacher C, Blume T, Beyer L, Peters F, Eckenweber F, Sgobio C, et al. Longitudinal PET monitoring of amyloidosis and microglial activation in a second-generation amyloid-beta mouse model. J Nucl Med. 2019;60(12):1787–93. https://doi.org/10.2967/jnumed.119.227322.
- 117. Biechele G, Wind K, Blume T, Sacher C, Beyer L, Eckenweber F, et al. Microglial activation in the right amygdala-entorhinal-hippocampal complex is associated with preserved spatial learning in App(NL-G-F) mice. Neuroimage. 2020;117707. https://doi.org/10.1016/j.neuroimage.2020.117707.
- 118. Serriere S, Tauber C, Vercouillie J, Mothes C, Pruckner C, Guilloteau D, et al. Amyloid load and translocator protein 18 kDa in APPswePS1-dE9 mice: a longitudinal study. Neurobiol Aging. 2015;36(4):1639–52. https://doi.org/10.1016/j.neurobiolaging.2014.11.023.
- 119. Chaney A, Bauer M, Bochicchio D, Smigova A, Kassiou M, Davies KE, et al. Longitudinal investigation of neuroinflammation and metabolite profiles in the APPswe xPS1Deltae9 transgenic mouse model of Alzheimer's disease. J Neurochem. 2018;144(3):318–35. https://doi.org/10.1111/jnc.14251.
- 120. Hu W, Pan D, Wang Y, Bao W, Zuo C, Guan Y, et al. PET imaging for dynamically monitoring neuroinflammation in APP/PS1 mouse model using [(18)F]DPA714. Front Neurosci. 2020;14:810. https://doi.org/10.3389/fnins.2020.00810.
- Levit A, Regis AM, Gibson A, Hough OH, Maheshwari S, Agca Y, et al. Impaired behavioural flexibility related to white matter microgliosis in the TgAPP21 rat model of Alzheimer disease. Brain Behav Immun. 2019;80:25–34. https://doi.org/10.1016/j.bbi.2019.02.013.
- 122. Weishaupt N, Liu Q, Shin S, Singh R, Agca Y, Agca C, et al. APP21 transgenic rats develop age-dependent cognitive impairment and microglia accumulation within white matter tracts. J Neuroinflammation. 2018;15(1):241. https://doi.org/10.1186/s12974-018-1273-7.
- 123. Yamagishi S, Iga Y, Nakamura M, Takizawa C, Fukumoto D, Kakiuchi T, et al. Upregulation of cannabinoid receptor type 2, but not TSPO, in senescence-accelerated neuroinflammation in mice: a positron emission tomography study. J Neuroinflammation. 2019;16(1):208. https://doi.org/10.1186/s12974-019-1604-3.
- 124. Tournier BB, Tsartsalis S, Rigaud D, Fossey C, Cailly T, Fabis F, et al. TSPO and amyloid deposits in sub-regions of the hippocampus in the 3xTgAD mouse model of Alzheimer's disease. Neurobiol Dis. 2019;121:95–105. https://doi.org/10.1016/j.nbd. 2018.09.022.
- Liu B, Hinshaw RG, Le KX, Park MA, Wang S, Belanger AP, et al. Space-like (56)Fe irradiation manifests mild, early sex-

- specific behavioral and neuropathological changes in wildtype and Alzheimer's-like transgenic mice. Sci Rep. 2019;9(1):12118. https://doi.org/10.1038/s41598-019-48615-1.
- Rowe CC, Ackerman U, Browne W, Mulligan R, Pike KL, O'Keefe G, et al. Imaging of amyloid beta in Alzheimer's disease with 18F-BAY94-9172, a novel PET tracer: proof of mechanism. Lancet Neurol. 2008;7(2):129–35. https://doi.org/10.1016/S1474-4422(08)70001-2.
- 127. Rominger A, Brendel M, Burgold S, Keppler K, Baumann K, Xiong G, et al. Longitudinal assessment of cerebral beta-amyloid deposition in mice overexpressing Swedish mutant beta-amyloid precursor protein using 18F-florbetaben PET. J Nucl Med. 2013;54(7):1127–34. https://doi.org/10.2967/jnumed. 112.114660.
- Saito T, Matsuba Y, Mihira N, Takano J, Nilsson P, Itohara S, et al. Single App knock-in mouse models of Alzheimer's disease. Nat Neurosci. 2014;17(5):661–3. https://doi.org/10.1038/nn. 3697.
- 129. Chen CJ, Bando K, Ashino H, Taguchi K, Shiraishi H, Shima K, et al. In vivo SPECT imaging of amyloid-beta deposition with radioiodinated imidazo[1,2-a]pyridine derivative DRM106 in a mouse model of Alzheimer's disease. J Nucl Med. 2015;56(1): 120–6. https://doi.org/10.2967/jnumed.114.146944.
- McGeer PL, Itagaki S, Boyes BE, McGeer EG. Reactive microglia are positive for HLA-DR in the substantia nigra of Parkinson's and Alzheimer's disease brains. Neurology. 1988;38(8):1285–91. https://doi.org/10.1212/wnl.38.8.1285.
- Tansey MG, Goldberg MS. Neuroinflammation in Parkinson's disease: its role in neuronal death and implications for therapeutic intervention. Neurobiol Dis. 2010;37(3):510–8. https://doi.org/10. 1016/j.nbd.2009.11.004.
- Cabezudo D, Baekelandt V, Lobbestael E. Multiple-hit hypothesis in Parkinson's disease: LRRK2 and inflammation. Front Neurosci. 2020;14:376. https://doi.org/10.3389/fnins.2020.00376.
- de Lau LM, Breteler MM. Epidemiology of Parkinson's disease.
 Lancet Neurol. 2006;5(6):525–35. https://doi.org/10.1016/S1474-4422(06)70471-9.
- Glass CK, Saijo K, Winner B, Marchetto MC, Gage FH. Mechanisms underlying inflammation in neurodegeneration. Cell. 2010;140(6):918–34. https://doi.org/10.1016/j.cell.2010. 02.016
- 135. Hatano K, Sekimata K, Yamada T, Abe J, Ito K, Ogawa M, et al. Radiosynthesis and in vivo evaluation of two imidazopyridineacetamides, [(11)C]CB184 and [(11)C]CB190, as a PET tracer for 18 kDa translocator protein: direct comparison with [(11)C](R)-PK11195. Ann Nucl Med. 2015;29(4):325–35. https://doi.org/10.1007/s12149-015-0948-8.
- 136. Rodriguez-Chinchilla T, Quiroga-Varela A, Molinet-Dronda F, Belloso-Iguerategui A, Merino-Galan L, Jimenez-Urbieta H, et al. [(18)F]-DPA-714 PET as a specific in vivo marker of early microglial activation in a rat model of progressive dopaminergic degeneration. Eur J Nucl Med Mol Imaging. 2020;47(11):2602–12. https://doi.org/10.1007/s00259-020-04772-4.
- 137. Wu CY, Chen YY, Lin JJ, Li JP, Chen JK, Hsieh TC, et al. Development of a novel radioligand for imaging 18-kD translocator protein (TSPO) in a rat model of Parkinson's disease. BMC Med Imaging. 2019;19(1):78. https://doi.org/10.1186/s12880-019-0375-8.
- Chen MK, Kuwabara H, Zhou Y, Adams RJ, Brasic JR, McGlothan JL, et al. VMAT2 and dopamine neuron loss in a primate model of Parkinson's disease. J Neurochem. 2008;105(1):78–90. https://doi.org/10.1111/j.1471-4159.2007. 05108 x.
- 139. Crabbe M, Van der Perren A, Bollaerts I, Kounelis S, Baekelandt V, Bormans G, et al. Increased P2X7 receptor binding is associated with neuroinflammation in acute but not chronic rodent



- models for Parkinson's disease. Front Neurosci. 2019;13:799. https://doi.org/10.3389/fnins.2019.00799.
- 140. Maia S, Arlicot N, Vierron E, Bodard S, Vergote J, Guilloteau D, et al. Longitudinal and parallel monitoring of neuroinflammation and neurodegeneration in a 6-hydroxydopamine rat model of Parkinson's disease. Synapse (New York, NY). 2012;66(7):573–83. https://doi.org/10.1002/syn.21543.
- 141. Vetel S, Serriere S, Vercouillie J, Vergote J, Chicheri G, Deloye JB, et al. Extensive exploration of a novel rat model of Parkinson's disease using partial 6-hydroxydopamine lesion of dopaminergic neurons suggests new therapeutic approaches. Synapse (New York, NY). 2019;73(3):e22077. https://doi.org/10.1002/syn. 22077.
- Belloli S, Morari M, Murtaj V, Valtorta S, Moresco RM, Gilardi MC. Translation imaging in Parkinson's disease: focus on neuro-inflammation. Front Aging Neurosci. 2020;12:152. https://doi.org/10.3389/fnagi.2020.00152.
- 143. Walsh S, Finn DP, Dowd E. Time-course of nigrostriatal neurodegeneration and neuroinflammation in the 6-hydroxydopamineinduced axonal and terminal lesion models of Parkinson's disease in the rat. Neuroscience. 2011;175:251–61. https://doi.org/10. 1016/j.neuroscience.2010.12.005.
- Cicchetti F, Brownell AL, Williams K, Chen YI, Livni E, Isacson O. Neuroinflammation of the nigrostriatal pathway during progressive 6-OHDA dopamine degeneration in rats monitored by immunohistochemistry and PET imaging. Eur J Neurosci. 2002;15(6):991–8. https://doi.org/10.1046/j.1460-9568.2002. 01938.x.
- 145. Fricke IB, Viel T, Worlitzer MM, Collmann FM, Vrachimis A, Faust A, et al. 6-hydroxydopamine-induced Parkinson's disease-like degeneration generates acute microgliosis and astrogliosis in the nigrostriatal system but no bioluminescence imaging-detectable alteration in adult neurogenesis. Eur J Neurosci. 2016;43(10):1352–65. https://doi.org/10.1111/ejn.13232.
- 146. Nomura M, Toyama H, Suzuki H, Yamada T, Hatano K, Wilson AA, et al. Peripheral benzodiazepine receptor/18 kDa translocator protein positron emission tomography imaging in a rat model of acute brain injury. Ann Nucl Med. 2021;35(1):8–16. https://doi.org/10.1007/s12149-020-01530-2.
- 147. Cumming P, Pedersen MD, Minuzzi L, Mezzomo K, Danielsen EH, Iversen P, et al. Distribution of PK11195 binding sites in porcine brain studied by autoradiography in vitro and by positron emission tomography. Synapse (New York, NY). 2006;59(7): 418–26. https://doi.org/10.1002/syn.20257.
- 148. Joers V, Masilamoni G, Kempf D, Weiss AR, Rotterman TM, Murray B, et al. Microglia, inflammation and gut microbiota responses in a progressive monkey model of Parkinson's disease: A case series. Neurobiol Dis. 2020;144:105027. https://doi.org/10. 1016/j.nbd.2020.105027.
- 149. Belloli S, Pannese M, Buonsanti C, Maiorino C, Di Grigoli G, Carpinelli A, et al. Early upregulation of 18-kDa translocator protein in response to acute neurodegenerative damage in TREM2deficient mice. Neurobiol Aging. 2017;53:159–68. https://doi.org/ 10.1016/j.neurobiolaging.2017.01.010.
- Lillethorup TP, Glud AN, Alstrup AKO, Mikkelsen TW, Nielsen EH, Zaer H, et al. Nigrostriatal proteasome inhibition impairs dopamine neurotransmission and motor function in minipigs. Exp Neurol. 2018;303:142–52. https://doi.org/10.1016/j.expneurol. 2018.02.005.
- Lillethorup TP, Glud AN, Alstrup AKO, Noer O, Nielsen EHT, Schacht AC, et al. Longitudinal monoaminergic PET imaging of chronic proteasome inhibition in minipigs. Sci Rep. 2018;8(1): 15715. https://doi.org/10.1038/s41598-018-34084-5.
- 152. Crabbe M, Van der Perren A, Kounelis S, Lavreys T, Bormans G, Baekelandt V, et al. Temporal changes in neuroinflammation and brain glucose metabolism in a rat model of viral vector-induced

- alpha-synucleinopathy. Exp Neurol. 2019;320:112964. https://doi.org/10.1016/j.expneurol.2019.112964.
- Lillethorup TP, Glud AN, Landeck N, Alstrup AKO, Jakobsen S, Vang K, et al. In vivo quantification of glial activation in minipigs overexpressing human alpha-synuclein. Synapse (New York, NY). 2018;72(12):e22060. https://doi.org/10.1002/syn.22060.
- 154. Walker MD, Dinelle K, Kornelsen R, Lee NV, Miao Q, Adam M, et al. [11C]PBR28 PET imaging is sensitive to neuroinflammation in the aged rat. J Cereb Blood Flow Metab. 2015;35(8):1331–8. https://doi.org/10.1038/jcbfm.2015.54.
- Shivers KY, Nikolopoulou A, Machlovi SI, Vallabhajosula S, Figueiredo-Pereira ME. PACAP27 prevents Parkinson-like neuronal loss and motor deficits but not microglia activation induced by prostaglandin J2. Biochim Biophys Acta. 2014;1842(9):1707– 19. https://doi.org/10.1016/j.bbadis.2014.06.020.
- Ghosh R, Tabrizi SJ. Clinical features of Huntington's disease.
 Adv Exp Med Biol. 2018;1049:1–28. https://doi.org/10.1007/978-3-319-71779-1
- 157. Tai YF, Pavese N, Gerhard A, Tabrizi SJ, Barker RA, Brooks DJ, et al. Microglial activation in presymptomatic Huntington's disease gene carriers. Brain. 2007;130(Pt 7):1759–66. https://doi.org/10.1093/brain/awm044.
- Singhrao SK, Neal JW, Morgan BP, Gasque P. Increased complement biosynthesis by microglia and complement activation on neurons in Huntington's disease. Exp Neurol. 1999;159(2):362

 76. https://doi.org/10.1006/expr.1999.7170.
- Dalrymple A, Wild EJ, Joubert R, Sathasivam K, Bjorkqvist M, Petersen A, et al. Proteomic profiling of plasma in Huntington's disease reveals neuroinflammatory activation and biomarker candidates. J Proteome Res. 2007;6(7):2833–40. https://doi.org/10. 1021/pr0700753.
- Pouladi MA, Morton AJ, Hayden MR. Choosing an animal model for the study of Huntington's disease. Nat Rev Neurosci. 2013;14(10):708–21. https://doi.org/10.1038/nrn3570.
- DiFiglia M. Excitotoxic injury of the neostriatum: a model for Huntington's disease. Trends Neurosci. 1990;13(7):286–9. https://doi.org/10.1016/0166-2236(90)90111-m.
- 162. Shear DA, Dong J, Gundy CD, Haik-Creguer KL, Dunbar GL. Comparison of intrastriatal injections of quinolinic acid and 3nitropropionic acid for use in animal models of Huntington's disease. Prog Neuro-Psychopharmacol Biol Psychiatry. 1998;22(7): 1217–40. https://doi.org/10.1016/s0278-5846(98)00070-0.
- 163. Brouillet E, Jacquard C, Bizat N, Blum D. 3-Nitropropionic acid: a mitochondrial toxin to uncover physiopathological mechanisms underlying striatal degeneration in Huntington's disease. J Neurochem. 2005;95(6):1521–40. https://doi.org/10.1111/j. 1471-4159.2005.03515.x.
- 164. Ferrante RJ, Kowall NW, Cipolloni PB, Storey E, Beal MF. Excitotoxin lesions in primates as a model for Huntington's disease: histopathologic and neurochemical characterization. Exp Neurol. 1993;119(1):46–71. https://doi.org/10.1006/exnr.1993. 1006.
- 165. Hantraye P, Riche D, Maziere M, Isacson O. A primate model of Huntington's disease: behavioral and anatomical studies of unilateral excitotoxic lesions of the caudate-putamen in the baboon. Exp Neurol. 1990;108(2):91–104. https://doi.org/10.1016/0014-4886(90)90014-i.
- Brouillet E, Conde F, Beal MF, Hantraye P. Replicating Huntington's disease phenotype in experimental animals. Prog Neurobiol. 1999;59(5):427–68. https://doi.org/10.1016/s0301-0082(99)00005-2.
- 167. Beal MF, Kowall NW, Ellison DW, Mazurek MF, Swartz KJ, Martin JB. Replication of the neurochemical characteristics of Huntington's disease by quinolinic acid. Nature. 1986;321(6066):168-71. https://doi.org/10.1038/321168a0.



- 168. Arlicot N, Katsifis A, Garreau L, Mattner F, Vergote J, Duval S, et al. Evaluation of CLINDE as potent translocator protein (18 kDa) SPECT radiotracer reflecting the degree of neuroinflammation in a rat model of microglial activation. Eur J Nucl Med Mol Imaging. 2008. https://doi.org/10.1007/s00259-008-0834-x.
- Beal MF, Ferrante RJ, Swartz KJ, Kowall NW. Chronic quinolinic acid lesions in rats closely resemble Huntington's disease. J Neurosci. 1991;11(6):1649–59.
- Ramachandran S, Thangarajan S. Thymoquinone loaded solid lipid nanoparticles counteracts 3-nitropropionic acid induced motor impairments and neuroinflammation in rat model of Huntington's disease. Metab Brain Dis. 2018;33(5):1459–70. https://doi.org/10. 1007/s11011-018-0252-0.
- Lavisse S, Inoue K, Jan C, Peyronneau MA, Petit F, Goutal S, et al. [18F]DPA-714 PET imaging of translocator protein TSPO (18 kDa) in the normal and excitotoxically-lesioned nonhuman primate brain. Eur J Nucl Med Mol Imaging. 2015;42(3):478–94. https://doi.org/10.1007/s00259-014-2962-9.
- 172. Arlicot N, Tronel C, Bodard S, Garreau L, de la Crompe B, Vandevelde I, et al. Translocator protein (18 kDa) mapping with [1251]-CLINDE in the quinolinic acid rat model of excitotoxicity: a longitudinal comparison with microglial activation, astrogliosis, and neuronal death. Mol Imaging. 2014;13:4–11.
- 173. Levivier M, Holemans S, Togasaki DM, Maloteaux JM, Brotchi J, Przedborski S. Quantitative assessment of quinolinic acid-induced striatal toxicity in rats using radioligand binding assays. Neurol Res. 1994;16(3):194–200. https://doi.org/10.1080/01616412. 1994.11740226.
- 174. Leaver KR, Reynolds A, Bodard S, Guilloteau D, Chalon S, Kassiou M. Effects of translocator protein (18 kDa) ligands on microglial activation and neuronal death in the quinolinic-acid-injected rat striatum. ACS Chem Neurosci. 2012;3(2):114–9. https://doi.org/10.1021/cn200099e.
- Ryu JK, Choi HB, McLarnon JG. Peripheral benzodiazepine receptor ligand PK11195 reduces microglial activation and neuronal death in quinolinic acid-injected rat striatum. Neurobiol Dis. 2005;20(2):550–61. https://doi.org/10.1016/j.nbd.2005.04.010.
- 176. Moresco RM, Lavazza T, Belloli S, Lecchi M, Pezzola A, Todde S, et al. Quinolinic acid induced neurodegeneration in the striatum: a combined in vivo and in vitro analysis of receptor changes and microglia activation. Eur J Nucl Med Mol Imaging. 2008;35(4): 704–15. https://doi.org/10.1007/s00259-007-0651-7.
- 177. Rojas S, Martin A, Arranz MJ, Pareto D, Purroy J, Verdaguer E, et al. Imaging brain inflammation with [(11)C]PK11195 by PET and induction of the peripheral-type benzodiazepine receptor after transient focal ischemia in rats. J Cereb Blood Flow Metab. 2007;27(12):1975–86. https://doi.org/10.1038/sj.jcbfm.9600500.
- Dusart I, Marty S, Peschanski M. Glial changes following an excitotoxic lesion in the CNS—II. Astrocytes. Neuroscience. 1991;45(3):541–9. https://doi.org/10.1016/0306-4522(91)90269-t.
- 179. Lavisse S, Guillermier M, Herard AS, Petit F, Delahaye M, Van Camp N, et al. Reactive astrocytes overexpress TSPO and are detected by TSPO positron emission tomography imaging. J Neurosci. 2012;32(32):10809–18. https://doi.org/10.1523/JNEUROSCI.1487-12.2012.
- Escartin C, Guillemaud O, Carrillo-de Sauvage MA. Questions and (some) answers on reactive astrocytes. Glia. 2019;67(12): 2221–47. https://doi.org/10.1002/glia.23687.
- Chang R, Liu X, Li S, Li XJ. Transgenic animal models for study of the pathogenesis of Huntington's disease and therapy. Drug Des Devel Ther. 2015;9:2179–88. https://doi.org/10.2147/DDDT. S58470
- 182. Davies SW, Turmaine M, Cozens BA, DiFiglia M, Sharp AH, Ross CA, et al. Formation of neuronal intranuclear inclusions underlies the neurological dysfunction in mice transgenic for the

- HD mutation. Cell. 1997;90(3):537–48. https://doi.org/10.1016/s0092-8674(00)80513-9.
- 183. Mangiarini L, Sathasivam K, Seller M, Cozens B, Harper A, Hetherington C, et al. Exon 1 of the HD gene with an expanded CAG repeat is sufficient to cause a progressive neurological phenotype in transgenic mice. Cell. 1996;87(3):493–506. https://doi.org/10.1016/s0092-8674(00)81369-0.
- 184. Luthi-Carter R, Hanson SA, Strand AD, Bergstrom DA, Chun W, Peters NL, et al. Dysregulation of gene expression in the R6/2 model of polyglutamine disease: parallel changes in muscle and brain. Hum Mol Genet. 2002;11(17):1911–26. https://doi.org/10. 1093/hmg/11.17.1911.
- 185. Hsiao HY, Chiu FL, Chen CM, Wu YR, Chen HM, Chen YC, et al. Inhibition of soluble tumor necrosis factor is therapeutic in Huntington's disease. Hum Mol Genet. 2014;23(16):4328–44. https://doi.org/10.1093/hmg/ddu151.
- Simmons DA, Casale M, Alcon B, Pham N, Narayan N, Lynch G. Ferritin accumulation in dystrophic microglia is an early event in the development of Huntington's disease. Glia. 2007;55(10): 1074–84. https://doi.org/10.1002/glia.20526.
- 187. Simmons DA, James ML, Belichenko NP, Semaan S, Condon C, Kuan J, et al. TSPO-PET imaging using [18F]PBR06 is a potential translatable biomarker for treatment response in Huntington's disease: preclinical evidence with the p75NTR ligand LM11A-31. Hum Mol Genet. 2018;27(16):2893–912. https://doi.org/10.1093/hmg/ddy202.
- 188. Mattner F, Staykova M, Berghofer P, Wong HJ, Fordham S, Callaghan P, et al. Central nervous system expression and PET imaging of the translocator protein in relapsing-remitting experimental autoimmune encephalomyelitis. J Nucl Med. 2013;54(2): 291–8. https://doi.org/10.2967/jnumed.112.108894.
- 189. Belloli S, Zanotti L, Murtaj V, Mazzon C, Di Grigoli G, Monterisi C, et al. (18)F-VC701-PET and MRI in the in vivo neuroinflammation assessment of a mouse model of multiple sclerosis. J Neuroinflammation. 2018;15(1):33. https://doi.org/10.1186/s12974-017-1044-x.
- Nack A, Brendel M, Nedelcu J, Daerr M, Nyamoya S, Beyer C et al. Expression of Translocator protein and [18F]-GE180 ligand uptake in multiple sclerosis animal models. Cells. 2019;8(2). doi: https://doi.org/10.3390/cells8020094.
- Vainio SK, Dickens AM, Tuisku J, Eskola O, Solin O, Loyttyniemi E, et al. Cessation of anti-VLA-4 therapy in a focal rat model of multiple sclerosis causes an increase in neuroinflammation. EJNMMI Res. 2019;9(1):38. https://doi.org/10.1186/ s13550-019-0508-7.
- Nedelcu J, Reinbach C, Riedler P, Brendel M, Rominger A, Kaye J, et al. Laquinimod ameliorates secondary brain inflammation. Neurobiol Dis. 2020;134:104675. https://doi.org/10.1016/j.nbd. 2019.104675.
- 193. Zinnhardt B, Belloy M, Fricke IB, Orije J, Guglielmetti C, Hermann S, et al. Molecular imaging of immune cell dynamics during de- and remyelination in the cuprizone model of multiple sclerosis by [(18)F]DPA-714 PET and MRI. Theranostics. 2019;9(6):1523–37. https://doi.org/10.7150/thno.32461.
- 194. Coda AR, Anzilotti S, Boscia F, Greco A, Panico M, Gargiulo S, et al. In vivo imaging of CNS microglial activation/macrophage infiltration with combined [(18)F]DPA-714-PET and SPIO-MRI in a mouse model of relapsing remitting experimental autoimmune encephalomyelitis. Eur J Nucl Med Mol Imaging. 2021;48(1):40–52. https://doi.org/10.1007/s00259-020-04842-7.
- Converse AK, Larsen EC, Engle JW, Barnhart TE, Nickles RJ, Duncan ID. 11C-(R)-PK11195 PET imaging of microglial activation and response to minocycline in zymosan-treated rats. J Nucl Med. 2011;52(2):257–62. https://doi.org/10.2967/jnumed.110. 082743.



- 196. Bruck W, Pfortner R, Pham T, Zhang J, Hayardeny L, Piryatinsky V, et al. Reduced astrocytic NF-kappaB activation by laquinimod protects from cuprizone-induced demyelination. Acta Neuropathol. 2012;124(3):411–24. https://doi.org/10.1007/s00401-012-1009-1.
- Thone J, Ellrichmann G, Seubert S, Peruga I, Lee DH, Conrad R, et al. Modulation of autoimmune demyelination by laquinimod via induction of brain-derived neurotrophic factor. Am J Pathol. 2012;180(1):267–74. https://doi.org/10.1016/j.ajpath.2011.09. 037
- 198. de Paula FD, de Vries EF, Sijbesma JW, Buchpiguel CA, Dierckx RA, Copray SC. PET imaging of glucose metabolism, neuroin-flammation and demyelination in the lysolecithin rat model for multiple sclerosis. Mult Scler. 2014;20(11):1443–52. https://doi.org/10.1177/1352458514526941.
- Martin A, Vazquez-Villoldo N, Gomez-Vallejo V, Padro D, Soria FN, Szczupak B, et al. In vivo imaging of system xc- as a novel approach to monitor multiple sclerosis. Eur J Nucl Med Mol Imaging. 2016;43(6):1124–38. https://doi.org/10.1007/s00259-015-3275-3.

- Wu C, Wang C, Popescu DC, Zhu W, Somoza EA, Zhu J, et al. A novel PET marker for in vivo quantification of myelination. Bioorg Med Chem. 2010;18(24):8592–9. https://doi.org/10.1016/j.bmc.2010.10.018.
- Chen Q, Meng X, McQuade P, Rubins D, Lin SA, Zeng Z, et al. Synthesis and preclinical evaluation of folate-NOTA-Al(18)F for PET Imaging of folate-receptor-positive tumors. Mol Pharm. 2016;13(5):1520–7. https://doi.org/10.1021/acs.molpharmaceut. 5b00989.
- 202. Elo P, Li XG, Liljenback H, Helin S, Teuho J, Koskensalo K, et al. Folate receptor-targeted positron emission tomography of experimental autoimmune encephalomyelitis in rats. J Neuroinflammation. 2019;16(1):252. https://doi.org/10.1186/s12974-019-1612-3.

Publisher's note Springer Nature remains neutral with regard to jurisdictional claims in published maps and institutional affiliations.

